NUMERICAL SOLUTION OF A SPATIO-TEMPORAL GENDER-STRUCTURED MODEL FOR HANTAVIRUS INFECTION IN RODENTS

RAIMUND BÜRGER

CI²MA and Departamento de Ingeniería Matemática, Universidad de Concepción,
Casilla 160-C, Concepción, Chile

GERARDO CHOWELL

School of Public Health, Georgia State University, Atlanta, Georgia, USA
Simon A. Levin Mathematical and Computational Modeling Sciences Center
Arizona State University, Tempe, AZ 85287, USA
Division of International Epidemiology and Population Studies,
Fogarty International Center, National Institutes of Health, Bethesda, MD 20892, USA

ELVIS GAVILÁN

CI²MA and Departamento de Ingeniería Matemática, Universidad de Concepción,
Casilla 160-C, Concepción, Chile

PEP MULET

Departament de Matemàtiques, Universitat de València
Av. Dr. Moliner 50, E-46100 Burjassot, Spain

LUIS M. VILLADA

GIMNAP-Departamento de Matemáticas, Universidad del Bío-Bío,
Casilla 5-C, Concepción, Chile
CI²MA, Universidad de Concepción, Casilla 160-C, Concepción, Chile

ABSTRACT. In this article we describe the transmission dynamics of hantavirus in rodents using a spatio-temporal susceptible-exposed-infective-recovered (SEIR) compartmental model that distinguishes between male and female subpopulations [L.J.S. Allen, R.K. McCormack and C.B. Jonsson, *Bull. Math. Biol.* **68** (2006), 511–524]. Both subpopulations are assumed to differ in their movement with respect to local variations in the densities of their own and the opposite gender group. Three alternative models for the movement of the male individuals are examined. In some cases the movement is not only directed by the gradient of a density (as in the standard diffusive case), but also by a nonlocal convolution of density values as proposed, in another context, in [R.M. Colombo and E. Rossi, *Commun. Math. Sci.*, **13** (2015), 369–400]. An efficient numerical method for the resulting convection-diffusion-reaction system of partial differential equations is proposed. This method involves techniques of

weighted essentially non-oscillatory (WENO) reconstructions in combination with implicit-explicit Runge-Kutta (IMEX-RK) methods for time stepping. The numerical results demonstrate significant differences in the spatio-temporal behavior predicted by the different models, which suggest future research directions.

1. Introduction.

1.1. **Scope.** Hantavirus (family Bunyaviridae) is a rodent-borne infectious disease of significant concern as it can generate high case fatality rates in the human population [55]. Transmission of hantavirus from infected rodents, the main known reservoir of the virus, to humans, typically occurs via inhalation of aerosols contaminated by virus shed in excreta, saliva, and urine [36]. Risk of infection with hantavirus in the human population is facilitated by crowding conditions and close proximity to rodent populations. Not surprisingly, the total population at risk for hantavirus infection has increased with urbanization rates. In the Americas, hantavirus represents a public health issue particularly in South American countries including Chile [48]. The great majority of hantavirus cases have been reported in China, however [64, 65]. A better understanding of the transmission dynamics of hantavirus in rodent populations has the potential to improve interventions strategies aimed at minimizing the number of infections in the human population.

It is the purpose of this contribution to advance a spatio-temporal compartmental model of hantavirus infection in rodents with a focus on its efficient numerical solution. The total population of rodents is subdivided into males and females (indices m and f), and for each of both subpopulations a variant of the well-known susceptible-exposed-infective-recovered (SEIR) compartmental model [33] is formulated. The compartments of male and female individuals are $\mathcal{C}_\mathrm{m} := \{S_\mathrm{m}, E_\mathrm{m}, I_\mathrm{m}, R_\mathrm{m}\}$ and $\mathcal{C}_\mathrm{f} := \{S_\mathrm{f}, E_\mathrm{f}, I_\mathrm{f}, R_\mathrm{f}\}$, respectively, and the final model for

$$\boldsymbol{u} = (u_1, \dots, u_8)^\mathrm{T} = (S_\mathrm{m}, E_\mathrm{m}, I_\mathrm{m}, R_\mathrm{m}, S_\mathrm{f}, E_\mathrm{f}, I_\mathrm{f}, R_\mathrm{f})^\mathrm{T}$$

as a function of position $\boldsymbol{x} \in \Omega$ and time $t \in \mathcal{T} := [0, T]$ on a bounded domain $\Omega \subset \mathbb{R}^2$ is given by a convection-diffusion-reaction system of the type

$$\frac{\partial \boldsymbol{u}}{\partial t} + \nabla \cdot \boldsymbol{F}^\mathrm{c}(\boldsymbol{u}) = \boldsymbol{\mathcal{D}} \Delta \boldsymbol{u} + \boldsymbol{s}(\boldsymbol{u}), \tag{1.1}$$

supplied with initial and boundary conditions, where the convective fluxes $\boldsymbol{F}^\mathrm{c}(\boldsymbol{u})$, the diffusion matrix $\boldsymbol{\mathcal{D}}$ and the vector of reaction terms $\boldsymbol{s}(\boldsymbol{u})$ are specified in later parts of the paper. It is proposed to describe the movement of the male individuals in a particular way that depends non-locally on the density $N_\mathrm{f} = S_\mathrm{f} + E_\mathrm{f} + I_\mathrm{f} + R_\mathrm{f}$ of female individuals, in combination with several alternative local or non-local dependences on the density $N_\mathrm{m} = S_\mathrm{m} + E_\mathrm{m} + I_\mathrm{m} + R_\mathrm{m}$ of male individuals. These alternatives give rise to three models that will be discussed in parallel, and that are expressed by the respective choice of $\boldsymbol{F}^\mathrm{c}(\boldsymbol{u})$. In any case the movement of the male individuals is assumed to depend non-locally on N_f. All variants of (1.1) call for numerical methods that on one hand avoid the severe time step restriction incurred by explicit time discretizations of the diffusion term $\boldsymbol{\mathcal{D}} \Delta \boldsymbol{u}$, and on the other hand allow the efficient computation of numerical fluxes based on the non-local evaluation of data. As we outline in this paper, the first goal can be achieved by an implicit-explicit (IMEX) discretization in combination with a technique based on Fast Fourier Transform (FFT) to handle the second. The simulator constructed in this way is applied to provide numerical results of several scenarios that allow comparing the model variants.

1.2. **Related work.** First of all, it worth mentioning that general references to the spatial spread of infectious diseases include [5,22,38,41,52,60]. The basic assumption of our treatment, namely that all epidemiological compartments are distributed over the whole spatial domain, is opposed to the alternative metapopulation approach that describes spatial structure through the relations between a number of well-identified sub-populations or "patches" (cf., e.g., [3, 6, 7, 18, 35, 57, 58]).

In fact, the description of spatial structure by explicitly specifying the mobilities between "patches" is typical for characterizing the behavior of humans, who usually do not "disperse" in response to environmental stimuli (at least not in the relatively short time scales involved in epidemiological modelling) but undertake directed travels, while a description through a convection-diffusion-reaction mechanism is more suitable for non-human infectious agents such as spores, insects, and bacteria that would disperse. The diffusion mechanism is mostly associated with non-human beings is also supported by the fact that classical treatments of diffusion in ecology only include non-human populations (cf. [41, Ch. 13], [43]). This viewpoint is also assumed, for instance, in [22, Ch. 10]. Other references to the movement of animals and spread of diseases by reaction-diffusion equations include [38, 44, 51]. Furthermore, the distinction between metapopulation models and continuous in space models is also made in the alternative treatments in Sections 4.3 and 4.4 of Sattenspiel [52] and those by van den Driessche [58] and Wu [61] in the same volume. In the latter, a decisive advantage of the spatially continuous approach, namely its amenability to mathematical analysis is emphasized. Furthermore, a reaction-diffusion system based on the well-known non-spatial SIR model [33] is proposed as a prototype spatio-temporal epidemic model, and the underlying assumptions of variants of reaction-diffusion models are broadly discussed, with particular reference to a seminal case study [29, 30, 42].

A less common ingredient in mathematical epidemiology is the convective term $\nabla \cdot \boldsymbol{F}^{\mathrm{c}}(\boldsymbol{u})$. Related advection terms, for which the essential functional dependence for one compartment is $\boldsymbol{F}^{\mathrm{c}} = \boldsymbol{F}^{\mathrm{c}}(\boldsymbol{x}, u) = \boldsymbol{b}(\boldsymbol{x})u$ with a given velocity $\boldsymbol{b}(\boldsymbol{x})$, arise if the population under study is transported (as is the case with wind-borne infectious agents, plankton, etc.). A slightly different motivation of convective terms was advanced in [41, Ch. 14] in the context of a wolf territoriality model that describes directed movement of individuals towards a "den". Surprisingly, however, nonlinear convective models are less common in epidemiological applications (although they are widespread used to describe human behavior of, say, traffic and pedestrian flows [26,28,56]). Let us emphasize here that the main role of the convective term in our model is similar to that of [41, Ch. 14] in that it imposes a preferred direction of movement of (the male) individuals, where the global dependence of the direction is determined by convolution with population data within a certain horizon of current position. This idea of non-local dependence of biological fluxes goes back to a non-local predator-prey model introduced and analyzed by Colombo and Rossi [20], and for which a numerical scheme is analyzed in [50]. The scheme proposed in that paper is based on the Lax-Friedrichs scheme for the (hyperbolic) equation (2.11a) for the ease of demonstrating convergence properties; we here employ higher-order weighted essentially non-oscillatory (WENO) reconstructions (initially proposed in [27, 37]) to achieve high-order spatial accuracy. (We will further relate our model to that of [20] in Section 2.3.)

Still within the framework of reaction-diffusion systems (but in simpler versions than considered here), a number of qualitative analyses of hantavirus models are

available. For instance, Abramson and Kenkre [1] advance a two-equation reaction-diffusion model that is a spatial equation of the well-known susceptible-infectious-susceptible (SIS) model (the assumed population of mice is not structured in any other way), and demonstrate that one single lumped parameter, the carrying capacity, essentially controls the dynamics of the system; moreover a spatial distribution of its value explains the formation and disappearance of "refugia", that is of habitat regions with favorable conditions that influence the spatio-temporal patterns of hantavirus [2, 34]. Furthermore, based on the Abramson and Kenkre model [1], Buceta et al. [17] study the the impact of seasonality on hantavirus, with the remarkable result that the alternation of seasons, each of which associated with a constant set of epidemiological parameters, may induce the outbreak of Hantavirus infection even if neither season by itself satisfies the environmental requirements for propagation of the disease [17]. The same group also investigated the effects of intrinsic noise on hantavirus spread [24]. Finally, we mention that more recently the Abramson and Kenkre model was refined to give a stage-dependent model with delay [46], where a new compartment corresponds to virus-free young mice, and the new model consists of three ordinary differential equations with delay, or in its recent spatial version presented in [47], in a reaction-diffusion system with delay (where the diffusion operator is expressed in radial variables).

From a computational point of view, and coming back to our own model (1.1), we mention that IMEX Runge-Kutta (IMEX-RK) schemes play an important role. We therefore briefly provide some background on these methods. Roughly speaking, an IMEX-RK method for a convection-diffusion-reaction equation of the type (1.1) consists of a Runge-Kutta scheme with an implicit discretization of the diffusive term combined with an explicit one for the convective and reactive terms. To introduce the main idea, we consider the problem

$$\frac{\mathrm{d}\boldsymbol{v}}{\mathrm{d}t} = \Phi^*(\boldsymbol{v}) + \Phi(\boldsymbol{v}), \tag{1.2}$$

which is assumed to represent a method-of-lines semi-discretization of (1.1), where $\Phi^*(\boldsymbol{v})$ and $\Phi(\boldsymbol{v})$ are spatial discretizations of the convective and reactive terms and of the diffusive term, respectively. Assume, for simplicity, that the spatial mesh width is $h > 0$ in both the x- and y-direction. Then the stability restriction on the time step Δt that explicit schemes impose when applied to (1.2) is very severe (Δt must be proportional to the square h^2 of the grid spacing), due to the presence of $\Phi(\boldsymbol{v})$. The implicit treatment of both $\Phi^*(\boldsymbol{v})$ and $\Phi(\boldsymbol{v})$ would remove any stability restriction on Δt. However, the upwind nonlinear discretization of the convective terms contained in $\Phi^*(\boldsymbol{v})$ that is needed for stability, makes its implicit treatment extremely involved. This situation becomes even more complicated due to the WENO reconstructions. In fact, after the pioneering work of Crouzeix [21], numerical integrators that deal implicitly with $\Phi(\boldsymbol{v})$ and explicitly with $\Phi^*(\boldsymbol{v})$ can be used with a time step restriction dictated by the convective-reactive term alone. These schemes, apart from having been profusely used in convection-diffusion problems and convection problems with stiff reaction terms [8, 23], have been recently used to deal with stiff terms in hyperbolic systems with relaxation (see [11–14, 45]). Finally, we mention that many authors have proposed IMEX-RK schemes for the solution of semi-discretized PDEs [8, 32, 45, 66].

1.3. **Outline of the paper.** The remainder of this work is organized as follows. The mathematical model is introduced in Section 2, starting from the spatio-temporal balance equations of a gender-structured SEIR model (in Section 2.1). The three variants of convective fluxes $\boldsymbol{F}^{\mathrm{c}}(\boldsymbol{u})$ and the diffusion matrix $\boldsymbol{\mathcal{D}}$ arising in (1.1) are specified in Section 2.2, and it is shown in Section 2.3 that the model arising from ours for N_{m} and N_{f} by summing over all compartments in C_{m} and C_{f}, respectively, can be compared with the non-local predator-prey model studied in [20]. In Section 3 we introduce the numerical scheme. We will use the method of lines to obtain a spatial semi-discretization of the initial-boundary value problem of (1.1) in the form of a system of ordinary differential equations (ODEs), to which a time-stepping procedure will be applied to obtain the final numerical scheme. To this end we introduce in Section 3.1 the Cartesian grid and discrete unknowns, and describe in Section 3.2 the discretization of non-local terms as in (2.6) that appear in the male convective fluxes. Then, in Section 3.3, we introduce the discretization of the the complete convective flux for the male species. This is essentially done by WENO reconstruction. The corresponding discretization for the female species is similar, and is omitted. Next, in Section 3.4 we describe the IMEX-RK time integrators used to solve the system of ODEs that represents the spatial discretization. Section 4 is devoted to the presentation of numerical results. Preliminaries are introduced in Section 4.1, including a definition of the constants arising in the model and of the initial scenarios. To make our results comparable with those of [4] (based on ordinary and stochastic differential equations), we adopt the parameters corresponding to the epizoology of the rice rat and the Bayou virus utilized in that paper. On the other hand, Scenario 1 is based on the hypothesis that the initial population occupies a well-identified subdomain of Ω and therefore the numerical results also address the phenomenon of biological invasion (besides that of the progression of epidemic states), while Scenario 2 aims at studying the effect of a random perturbation of a constant initial state. The corresponding numerical examples are presented in Sections 4.2 and 4.3, respectively. Furthermore, we provide in Section 4.4 an example that shows that the numerical scheme exhibits experimental second-order convergence when the solution is smooth, and in Section 4.5 present a test case that addresses the effect of seasonal variability of some of the model parameters. Conclusions are collected in Section 5.

2. Mathematical model.

2.1. **Gender-structured spatio-temporal SEIR model.** The model for the eight unknowns in $\mathcal{C} := \mathcal{C}_{\mathrm{m}} \cup \mathcal{C}_{\mathrm{f}}$, as functions of $\boldsymbol{x}$ and t, is given as follows:

$$\frac{\partial S_{\mathrm{m}}}{\partial t} + \nabla \cdot F_{S_{\mathrm{m}}}(S_{\mathrm{m}}, N_{\mathrm{f}}, N_{\mathrm{m}}) = \frac{B(N_{\mathrm{m}}, N_{\mathrm{f}})}{2} - S_{\mathrm{m}} d(N) - S_{\mathrm{m}}(\beta_{\mathrm{f}} I_{\mathrm{f}} + \beta_{\mathrm{m}} I_{\mathrm{m}}), \quad (2.1\mathrm{a})$$

$$\frac{\partial E_{\mathrm{m}}}{\partial t} + \nabla \cdot F_{E_{\mathrm{m}}}(E_{\mathrm{m}}, N_{\mathrm{f}}, N_{\mathrm{m}}) = -E_{\mathrm{m}} d(N) + S_{\mathrm{m}}(\beta_{\mathrm{f}} I_{\mathrm{f}} + \beta_{\mathrm{m}} I_{\mathrm{m}}) - \delta E_{\mathrm{m}}, \quad (2.1\mathrm{b})$$

$$\frac{\partial I_{\mathrm{m}}}{\partial t} + \nabla \cdot F_{I_{\mathrm{m}}}(I_{\mathrm{m}}, N_{\mathrm{f}}, N_{\mathrm{m}}) = \delta E_{\mathrm{m}} - I_{\mathrm{m}} d(N) - \gamma_{\mathrm{m}} I_{\mathrm{m}}, \quad (2.1\mathrm{c})$$

$$\frac{\partial R_{\mathrm{m}}}{\partial t} + \nabla \cdot F_{R_{\mathrm{m}}}(R_{\mathrm{m}}, N_{\mathrm{f}}, N_{\mathrm{m}}) = \gamma_{\mathrm{m}} I_{\mathrm{m}} - R_{\mathrm{m}} d(N), \quad (2.1\mathrm{d})$$

$$\frac{\partial S_{\mathrm{f}}}{\partial t} - \nabla \cdot \left(\mu_{S_{\mathrm{f}}} \nabla S_{\mathrm{f}}\right) = \frac{B(N_{\mathrm{m}}, N_{\mathrm{f}})}{2} - S_{\mathrm{f}} d(N) - S_{\mathrm{f}}(\beta_{\mathrm{f}} I_{\mathrm{f}} + \beta_{\mathrm{m,f}} I_{\mathrm{m}}), \quad (2.1\mathrm{e})$$

$$\frac{\partial E_{\mathrm{f}}}{\partial t} - \nabla \cdot \left(\mu_{E_{\mathrm{f}}} \nabla E_{\mathrm{f}}\right) = -E_{\mathrm{f}} d(N) + S_{\mathrm{f}}(\beta_{\mathrm{f}} I_{\mathrm{f}} + \beta_{\mathrm{m,f}} I_{\mathrm{m}}) - \delta E_{\mathrm{f}}, \quad (2.1\mathrm{f})$$

$$\frac{\partial I_f}{\partial t} - \nabla \cdot \left(\mu_{I_f} \nabla I_f \right) = \delta E_f - I_f d(N) - \gamma_f I_f, \tag{2.1g}$$

$$\frac{\partial R_f}{\partial t} - \nabla \cdot \left(\mu_{R_f} \nabla R_f \right) = \gamma_f I_f - R_f d(N), \tag{2.1h}$$

where $\nabla \cdot$ denotes the (spatial) divergence operator. The right-hand sides of (2.1) are identical to that of the non-spatial model proposed in [4], i.e., this model, to which we refer as Model 0 for ease of reference, is recovered if all divergence terms on the left-hand sides are set to zero and variables are considered to depend on t only, and the unknowns represent suitably scaled densities. In particular $d(N)$ is the density-dependent death rate, β_f is the contact rate of an infective female with either a susceptible female or a susceptible male, $\beta_{m,f}$ is the contact rate of an infective male with a susceptible female, β_m is the contact rate of an infective male with a susceptible male, δ is the inverse of the average length of the incubation period (assumed to be the same for males and females), and γ_m and γ_f are the inverse of average length of the infectious periods for males and females, respectively. Following [4], we assume a harmonic birth function,

$$B(N_m, N_f) = \frac{2bN_m N_f}{N_m + N_f},$$

where b is the average litter size, and regarding the contact rates and infectious periods, we assume $\beta_m \geq \beta_{m,f} \geq \beta_f$ and $\gamma_f > \gamma_m$. The incubation period is the same for males and females (namely $1/\delta$), as is the density-dependent death rate

$$d(N) = a + cN,$$

where $0 < a < b/2$ and $c > 0$.

2.2. **Convective fluxes and diffusion matrix.** The fluxes appearing in the left-hand sides of the full spatio-temporal model (2.1) have two components for the male compartments, and one for the female compartments. Several alternative choices of F_X for the males in compartment $X \in \mathcal{C}_m$ will be considered in parallel and compared. Model 1 is given by (2.1) along with

$$F_X(X, N_f, N_m) = X\left(\kappa_X \boldsymbol{V}(N_f) - \mu_X \boldsymbol{V}(N_m) \right), \tag{2.2}$$

where $\kappa_X \geq 0$ and $\mu_X \geq 0$ are constants and $\boldsymbol{V}$ is a non-local velocity function that will be specified below. Model 2 is given by (2.1) in combination with

$$F_X(X, N_f, N_m) = X\varphi(N_m + N_f)\left(\kappa_X \boldsymbol{V}(N_f) - \mu_X \boldsymbol{V}(N_m) \right), \tag{2.3}$$

where the function φ is given by

$$\varphi(u) = \begin{cases} 1 - u/K & \text{for } 0 \leq u \leq K, \\ 0 & \text{for } u < 0 \text{ or } u > K, \end{cases} \tag{2.4}$$

where K is a maximum value (carrying capacity) of the total density. Finally, we consider Model 3 that is given by

$$F_X(X, N_f, N_m) = X\kappa_X \boldsymbol{V}(N_f) - \mu_X \nabla X, \tag{2.5}$$

where ∇X is the spatial gradient of X.

The non-local unscaled velocity $\boldsymbol{V}$ is defined as

$$\boldsymbol{V}(w) = \frac{\nabla(w * \eta)}{\sqrt{1 + \|\nabla(w * \eta)\|^2}}, \tag{2.6}$$

where η denotes a radial convolution kernel with radius ε, i.e., η is a piecewise smooth function such that $\eta(\boldsymbol{x}) = \eta(\|\boldsymbol{x}\|_2)$, $\eta(\boldsymbol{x}) \geq 0$, $\eta(\boldsymbol{x}) = 0$ for $\|\boldsymbol{x}\| > \varepsilon$, and $\int_{\mathbb{R}^2} \eta(\boldsymbol{x})\,\mathrm{d}\boldsymbol{x} = 1$, i.e., for any function w defined on $\Omega \times \mathcal{T}$ and $\boldsymbol{x} \in \Omega$ such that $B_\varepsilon(\boldsymbol{x}) := \{\boldsymbol{y} \in \mathbb{R}^2 : \|\boldsymbol{y} - \boldsymbol{x}\| < \varepsilon\} \subset \Omega$, we have

$$(w(\cdot,t) * \eta)(\boldsymbol{x}) = \int_{B_\varepsilon(\boldsymbol{x})} w(\boldsymbol{y},t)\eta(\boldsymbol{x} - \boldsymbol{y})\,\mathrm{d}\boldsymbol{y} = \int_{\mathbb{R}^2} w(\boldsymbol{y},t)\eta(\boldsymbol{x} - \boldsymbol{y})\,\mathrm{d}\boldsymbol{y}.$$

(This definition will be modified slightly for points $\boldsymbol{x}$ with $\mathrm{dist}(\boldsymbol{x}, \partial\Omega) < \varepsilon$.) It is worth recalling that

$$\nabla(w * \eta) = w * \nabla\eta, \tag{2.7}$$

so that $\boldsymbol{V}(w)$ indeed depends (non-locally) on w and not on its gradient.

The non-local velocity function (2.6) was introduced recently in a two-species predator-prey model by Colombo and Rossi [20], for which convergence of a numerical scheme was proved by Rossi and Schleper [50]. The evaluation of this velocity function at $w = N_{\mathrm{f}}$ in the equations for male individuals describes that males are attracted by females since the corresponding biological fluxes $\kappa_C \boldsymbol{V}(N_{\mathrm{f}})$, $C \in \mathcal{C}_{\mathrm{m}}$, are directed toward increasing densities of females. The movement of male individuals to females is balanced by a term that describes that males avoid groups of their own gender. This is achieved in Models 1 and 2 by another evaluation of the nonlocal function but this time at $w = N_{\mathrm{m}}$, and with a coefficient, namely $-\mu_X$, of opposite sign (see (2.2) and (2.3)), while in Model 3 the movement of males away from regions of large densities of their group is described by diffusive movement through the term $-\mu_X \nabla X$ (see (2.5)). The biological movement of females is standard diffusion.

Summarizing, we obtain that the convective fluxes $\boldsymbol{F}^{\mathrm{c}}(\boldsymbol{u})$ and the diffusion matrix $\boldsymbol{\mathcal{D}}$ arising in (1.1) are given by the respective expressions

$$\boldsymbol{F}^{\mathrm{c}}(\boldsymbol{u}) = \big(F_{S_{\mathrm{m}}}(S_{\mathrm{m}}, N_{\mathrm{f}}, N_{\mathrm{m}}), F_{E_{\mathrm{m}}}(E_{\mathrm{m}}, N_{\mathrm{f}}, N_{\mathrm{m}}), F_{I_{\mathrm{m}}}(I_{\mathrm{m}}, N_{\mathrm{f}}, N_{\mathrm{m}}),$$
$$F_{R_{\mathrm{m}}}(R_{\mathrm{m}}, N_{\mathrm{f}}, N_{\mathrm{m}}), 0, 0, 0, 0\big)^{\mathrm{T}},$$
$$\boldsymbol{\mathcal{D}} = \mathrm{diag}(0, 0, 0, 0, \mu_{S_{\mathrm{f}}}, \mu_{E_{\mathrm{f}}}, \mu_{I_{\mathrm{f}}}, \mu_{R_{\mathrm{f}}}),$$

when the definition of the fluxes is (2.2) (Model 1) or (2.3) , (2.4) (Model 2), and

$$\boldsymbol{F}^{\mathrm{c}}(\boldsymbol{u}) = \big(S_{\mathrm{m}}\kappa_{S_{\mathrm{m}}}\boldsymbol{V}(N_{\mathrm{f}}), E_{\mathrm{m}}\kappa_{E_{\mathrm{m}}}\boldsymbol{V}(N_{\mathrm{f}}), I_{\mathrm{m}}\kappa_{I_{\mathrm{m}}}\boldsymbol{V}(N_{\mathrm{f}}),$$
$$R_{\mathrm{m}}\kappa_{R_{\mathrm{m}}}\boldsymbol{V}(N_{\mathrm{f}}), 0, 0, 0, 0\big)^{\mathrm{T}}, \tag{2.8}$$
$$\boldsymbol{\mathcal{D}} = \mathrm{diag}(\mu_{S_{\mathrm{m}}}, \mu_{E_{\mathrm{m}}}, \mu_{I_{\mathrm{m}}}, \mu_{R_{\mathrm{m}}}, \mu_{S_{\mathrm{f}}}, \mu_{E_{\mathrm{f}}}, \mu_{I_{\mathrm{f}}}, \mu_{R_{\mathrm{f}}}),$$

for the definition of the fluxes (2.5) (Model 3). In all cases, the vector of reaction terms $\boldsymbol{s}(\boldsymbol{u}) = (s_1(\boldsymbol{u}), \ldots, s_8(\boldsymbol{u}))^{\mathrm{T}}$ is given by the right-hand sides of (2.1), i.e.,

$$s_1(\boldsymbol{u}) = \frac{B(N_{\mathrm{m}}, N_{\mathrm{f}})}{2} - S_{\mathrm{m}}d(N) - S_{\mathrm{m}}(\beta_{\mathrm{f}}I_{\mathrm{f}} + \beta_{\mathrm{m}}I_{\mathrm{m}}), \ldots, s_8(\boldsymbol{u}) = \gamma_{\mathrm{f}}I_{\mathrm{f}} - R_{\mathrm{f}}d(N).$$

The system (2.1) is considered on $\Omega \times \mathcal{T}$ together with the initial condition

$$\boldsymbol{u}(\boldsymbol{x}, 0) = \boldsymbol{u}_0(\boldsymbol{x}), \quad \boldsymbol{x} \in \Omega, \tag{2.9}$$

where $\boldsymbol{u}_0$ is a given function, and zero-flux boundary conditions

$$\big(\boldsymbol{F}^{\mathrm{c}}(\boldsymbol{u}) - \boldsymbol{\mathcal{D}}\nabla\boldsymbol{u}\big) \cdot \boldsymbol{n} = \boldsymbol{0}, \quad \boldsymbol{x} \in \partial\Omega, \quad t \in (0, T], \tag{2.10}$$

where $\boldsymbol{n}$ is the unit exterior normal vector to the boundary $\partial\Omega$ of Ω.

2.3. Comparison with the model by Colombo and Rossi [20]. Assume that the convective fluxes $\boldsymbol{F}^{\mathrm{c}}(\boldsymbol{u})$ and the diffusion matrix $\boldsymbol{D}$ are given by (2.8) according to Model 3, and that $\kappa_C = \kappa_{\mathrm{m}}$ and $\mu_C = \mu_{\mathrm{m}}$ for all $C \in \mathcal{C}_{\mathrm{m}}$ and $\mu_C = \mu_{\mathrm{f}}$ for all $C \in \mathcal{C}_{\mathrm{f}}$. Then, summing (2.1a)–(2.1d) and (2.1e)–(2.1h), respectively, we get the two equations

$$\frac{\partial N_{\mathrm{m}}}{\partial t} + \nabla \cdot \left(\kappa_{\mathrm{m}} N_{\mathrm{m}} \boldsymbol{V}(N_{\mathrm{f}}) - \mu_{\mathrm{m}} \nabla N_{\mathrm{m}}\right) = \frac{B(N_{\mathrm{m}}, N_{\mathrm{f}})}{2} - N_{\mathrm{m}} d(N_{\mathrm{m}} + N_{\mathrm{f}}), \quad (2.11\mathrm{a})$$

$$\frac{\partial N_{\mathrm{f}}}{\partial t} - \mu_{\mathrm{f}} \Delta N_{\mathrm{f}} = \frac{B(N_{\mathrm{m}}, N_{\mathrm{f}})}{2} - N_{\mathrm{f}} d(N_{\mathrm{m}} + N_{\mathrm{f}}). \quad (2.11\mathrm{b})$$

This model is similar to the non-local predator-prey model recently analyzed by Colombo and Rossi [20]. In fact, their model is precisely recovered if we identify N_{m} as the density of "predators", N_{f} as that of "prey", set $\kappa_{\mathrm{m}} = 1$ and $\mu_{\mathrm{m}} = 0$, and replace the right-hand sides of (2.11a) and (2.11b) by the respective expressions $(\alpha N_{\mathrm{f}} - \beta) N_{\mathrm{m}}$ and $(\gamma - \delta N_{\mathrm{m}}) N_{\mathrm{f}}$, with positive constants $\alpha, \beta, \gamma, \delta$, of the well-known Lotka-Volterra predator-prey kinetics [15].

3. Numerical scheme.

3.1. Discretization of local convection and diffusion terms. We take $\Omega = [0, L] \times [0, L]$ and use a Cartesian grid with nodes (x_i, y_j), $i, j = 1, \ldots, M$, with $x_i = y_i = (i - 1/2)h$, $h = L/M$.

We discretize $\nabla \cdot \boldsymbol{F}^{\mathrm{c}}(\boldsymbol{u})$ on this grid by weighted essentially non-oscillatory (WENO) finite differences and $\Delta \boldsymbol{u}$ by the standard second-order scheme with a five-point stencil to get a spatial semi-discretization of (1.1) for an $8 \times M \times M$-matrix $\boldsymbol{v}(t)$ of unknown approximations

$$\boldsymbol{v}_{\ell,i,j}(t) \approx u_\ell(x_i, y_j, t), \quad i, j = 1, \ldots, M, \quad \ell = 1, \ldots, 8$$

given by

$$\boldsymbol{v}' = -\nabla_h \cdot \widetilde{\boldsymbol{F}}^{\mathrm{c}}(\boldsymbol{v}) + \boldsymbol{\mathcal{B}}\boldsymbol{v} + \boldsymbol{S}(\boldsymbol{v}), \quad (3.1)$$

to which suitable implicit-explicit Runge-Kutta (IMEX-RK) schemes will be applied for obtaining the final fully-discrete scheme (see Section 3.4). In this equation $\nabla_h \cdot \widetilde{\boldsymbol{F}}^{\mathrm{c}}(\boldsymbol{v})$ is the discretization of $\nabla \cdot \boldsymbol{F}^{\mathrm{c}}(\boldsymbol{u})$, to be defined in Section 3.3, and

$$(\boldsymbol{\mathcal{B}}\boldsymbol{v})_{\ell,i,j} = \mu_\ell (\boldsymbol{\Delta}_h \boldsymbol{v}_\ell)_{i,j}, \quad i, j = 1, \ldots, M, \quad \ell = 1, \ldots, 8 \quad (3.2)$$

is the discretization of the diffusion terms. Notice that we take $\mu_\ell = 0$ for $\ell \in \{1, 2, 3, 4\}$ and models (2.2) or (2.3), for these models do not have diffusion for male species. Here we have used the notation $\boldsymbol{v}_\ell$ for the $M \times M$ submatrix given by $(\boldsymbol{v}_\ell)_{i,j} = \boldsymbol{v}_{\ell,i,j}$ and $\boldsymbol{\Delta}_h$ for the standard two-dimensional Laplacian operator with Neumann boundary conditions. Furthermore, $\boldsymbol{S}(\boldsymbol{v})$ is the $8 \times M \times M$-matrix with components

$$\boldsymbol{S}(\boldsymbol{v})_{\ell,i,j} = s_\ell(\boldsymbol{v}_{\ell,i,j}), \quad i, j = 1, \ldots, M, \quad \ell = 1, \ldots, 8,$$

with corresponding submatrices $\boldsymbol{S}_\ell(\boldsymbol{v})$, given by

$$\boldsymbol{S}_\ell(\boldsymbol{v})_{i,j} = s_\ell(\boldsymbol{v}_{\ell,i,j}). \quad (3.3)$$

We explain the discretization of the convective term appearing in (3.1) in the next two subsections.

3.2. **Discretization of the convolutions.** We will use the following identity for the implementation that arises from (2.6) if we take into account (2.7):

$$\boldsymbol{V}(w) = \frac{w * \boldsymbol{\nu}}{\sqrt{1 + \|w * \nu\|^2}}, \quad \boldsymbol{\nu} = \left(\frac{\partial\eta}{\partial x}, \frac{\partial\eta}{\partial y}\right). \tag{3.4}$$

The convolutions $w * \chi$, $\chi = \partial\eta/\partial x$ or $\chi = \partial\eta/\partial y$, namely

$$(w * \chi)(\boldsymbol{x}) = \int_{B_\varepsilon(0)} w(\boldsymbol{x} - \boldsymbol{y})\chi(\boldsymbol{y})\,\mathrm{d}\boldsymbol{y},$$

are calculated approximately on the discrete grid via a composite Newton-Cotes quadrature formula, such as the composite Simpson rule.

Since $B_\varepsilon(0) \subseteq [-rh, rh]^2$, $r = \lceil\varepsilon/h\rceil < M$, and considering that, according to boundary conditions, w is extended to the exterior of Ω by reflection, e.g. by setting $w(-x, y) = w(x, y)$, $(x, y) \in \Omega$, we obtain

$$(w * \chi)(x_i, y_j) = \int_{-rh}^{rh} \int_{-rh}^{rh} w(x_i - x, y_j - y)\chi(x, y)\,\mathrm{d}x\,\mathrm{d}y$$

$$\approx h^2 \sum_{p=-r}^{r} \sum_{q=-r}^{r} \alpha_p\alpha_q w(x_i - x_p, y_j - y_q)\chi(x_p, y_q),$$

where α_p and α_q are the coefficients in the quadrature rule (e.g., for the composite Simpson rule, $\boldsymbol{\alpha} = (1, 4, 2, 4, \ldots, 2, 4, 1)$). This can be written as

$$(w * \chi)(x_i, y_j) \approx \sum_{p=-r}^{r} \sum_{q=-r}^{r} \beta_{p,q} w(x_{i-p}, y_{j-q}), \quad \beta_{p,q} = h^2\alpha_p\alpha_q\chi(x_p, y_q). \tag{3.5}$$

The accuracy order of this approximation is given by that of the quadrature rule, e.g., it is fourth-order accurate for the composite Simpson rule. Consequently, the approximation (3.5) for $\boldsymbol{W} = (w_{i,j}) \in \mathbb{R}^{M \times M}$, $w_{i,j} \approx w(x_i, y_j)$, is given by

$$(w * \chi)(x_i, y_j) \approx (\boldsymbol{W} *_h \beta)_{i,j} := \sum_{p=-r}^{r} \sum_{q=-r}^{r} \beta_{p,q} w_{[i-p]_M, [j-q]_M}, \tag{3.6}$$

where we define

$$[i]_M := \begin{cases} -i+1 & \text{for } -r+1 \le i \le 0, \\ i & \text{for } 1 \le i \le M, \\ 2M+1-i & \text{for } M+1 \le i \le M+r. \end{cases}$$

The discrete approximation of $\boldsymbol{V}(w)$ in (3.4) obtained from the approximation $\boldsymbol{W} \approx w$ is given by

$$\boldsymbol{V}_h(\boldsymbol{W}) = \frac{\boldsymbol{W} *_h \boldsymbol{\nu}}{\sqrt{1 + \|\boldsymbol{W} *_h \nu\|^2}}, \quad \boldsymbol{\nu} = \left(\frac{\partial\eta}{\partial x}, \frac{\partial\eta}{\partial y}\right).$$

Since $r \approx \varepsilon/h = \varepsilon M/L$, the computational cost of this discrete convolution is $M^2(2r+1)^2 \approx 4\varepsilon^2 M^4/L^2$, which can be very high for large M. This cost can be substantially reduced to $\mathcal{O}(M^2 \log M)$ by performing a convolution with periodic data by Fast Fourier Transforms (FFTs) (see [31, 54]). To achieve this goal, we define from $\boldsymbol{W} = (w_{i,j}) \in \mathbb{R}^{M \times M}$ a matrix $\widetilde{\boldsymbol{W}} = (\tilde{w}_{i,j}) \in \mathbb{R}^{2M \times 2M}$ such that

$$\tilde{w}_{i,j} = w_{[i]_M, [j]_M}, \quad i, j = 1, \ldots, 2M$$

and use the notation $[i]'_{2M} = \mod(i-1, 2M) + 1$, i.e., $[i]'_{2M} = i + 2kM$, with k being the integer such that $1 \leq [i]'_{2M} \leq 2M$. With this notation it is readily checked that

$$w_{[i]_M, [j]_M} = \tilde{w}_{[i]'_{2M}, [j]'_{2M}}, \quad i, j = -r+1, \ldots, M+r.$$

Therefore (3.6) for $i, j = 1, \ldots, M$ can be rewritten as

$$(\boldsymbol{W} *_h \beta)_{i,j} = \sum_{p=-r}^{r} \sum_{q=-r}^{r} \beta_{p,q} \tilde{w}_{[i-p]'_{2M}, [j-q]'_{2M}}. \tag{3.7}$$

The convolution on the right-hand side of (3.7) can be performed by FFTs applied to the $(2M) \times (2M)$ matrix $\widetilde{\boldsymbol{W}}$. To save further computational costs, the FFT of the kernel $\beta_{p,q}$ is performed only once, son each convolution entails two two-dimensional FFT of $(2M) \times (2M)$ matrices and a product of $4M^2$ numbers, with an overall computational cost of $\mathcal{O}(M^2 \log M)$.

3.3. **Discretization of the convective term.** The convective flux for the ℓ (fe-male) species, $\ell \in \{5, 6, 7, 8\}$, is zero and the convective flux for the ℓ (male) species, $\ell \in \{1, 2, 3, 4\}$, in e.g., model (2.2) is given by

$$\boldsymbol{F}_\ell^c(\boldsymbol{u}) = \boldsymbol{u}_\ell\big(\kappa_\ell \boldsymbol{V}(u_5 + u_6 + u_7 + u_8) - \mu_\ell \boldsymbol{V}(u_1 + u_2 + u_3 + u_4)\big).$$

To discretize its divergence $\nabla \cdot \boldsymbol{F}_\ell^c(\boldsymbol{u})$, for the approximation $\boldsymbol{v}$, we first approximate the convolution terms as expounded in Section 3.2 to obtain

$$\widetilde{\boldsymbol{F}}_\ell^c(\boldsymbol{v})_{i,j} = \boldsymbol{v}_{\ell,i,j}\big(\kappa_\ell \boldsymbol{V}_h(v_5 + v_6 + v_7 + v_8)_{i,j} - \mu_\ell \boldsymbol{V}_h(v_1 + v_2 + v_3 + v_4)_{i,j}\big) \in \mathbb{R}^2.$$

Similar arguments are carried out for the other models (2.3) and (2.5).

We introduce the following notation:

$$\big(f_{i,j}^x, f_{i,j}^y\big) := \widetilde{\boldsymbol{F}}_\ell^c(\boldsymbol{v})_{i,j},$$

where we have dropped the ℓ index for obtaining clearer expressions.

Our purpose is to use a fifth-order WENO finite difference discretization [27, 37, 53] of $\nabla \cdot \boldsymbol{F}_\ell^c(\boldsymbol{u})$ for which

$$\nabla \cdot \boldsymbol{F}_\ell^c(\boldsymbol{u})(x_i, y_j)$$
$$\approx \nabla_h \cdot \tilde{\boldsymbol{F}}^c(\boldsymbol{v})_{\ell,i,j} := \frac{\hat{f}_{i+1/2,j}^x - \hat{f}_{i-1/2,j}^x}{h} + \frac{\hat{f}_{i,j+1/2}^y - \hat{f}_{i,j-1/2}^y}{h}, \tag{3.8}$$

for suitable numerical fluxes $\hat{f}_{i+1/2,j}^x, \hat{f}_{i,j+1/2}^y$ obtained by WENO reconstructions of split fluxes. For the numerical flux in the x-direction, the Lax-Friedrichs-type flux splitting $f^{x,\pm}$ is given by

$$f_{i,j}^{x,\pm} = \frac{1}{2}\big(f_{i,j}^x \pm \alpha^x v_{\ell,i,j}\big), \quad \alpha^x = \max_{i,j}|\boldsymbol{V}_h^x(\boldsymbol{v})_{i,j}|.$$

Likewise, the numerical flux $\hat{f}_{i,j+1/2}^y$ is obtained by WENO reconstructions of split fluxes given by

$$f_{i,j}^{y,\pm} = \frac{1}{2}\big(f_{i,j}^y \pm \alpha^y v_{\ell,i,j}\big), \quad \alpha^y = \max_{i,j}|\boldsymbol{V}_h^y(\boldsymbol{v})_{i,j}|.$$

If $\mathcal{R}^\pm$ denotes fifth-order WENO upwind biased reconstructions, then

$$\hat{f}_{i+1/2,j}^x = \mathcal{R}^+\big(f_{i-2:i+2,j}^{x,+}\big) + \mathcal{R}^-\big(f_{i-1:i+3,j}^{x,-}\big),$$
$$\hat{f}_{i,j+1/2}^y = \mathcal{R}^+\big(f_{i,j-2:j+2}^{y,+}\big) + \mathcal{R}^-\big(f_{i,j-1:j+3}^{y,-}\big),$$

where we have used matlab-type notation for submatrices.

3.4. **Implicit-explicit Runge-Kutta schemes.** We will use IMEX-RK integrators for ODEs, for which only the diffusion term will be treated implicitly, so we rewrite (3.1) as (1.2), where

$$\Phi^*(\boldsymbol{v}) := -\nabla_h \cdot \widetilde{\boldsymbol{F}}^{\mathrm{c}}(\boldsymbol{v}) + \boldsymbol{S}(\boldsymbol{v}), \qquad \Phi(\boldsymbol{v}) := \boldsymbol{\mathcal{B}}\boldsymbol{v}. \tag{3.9}$$

For the diffusive part $\Phi(\boldsymbol{v})$ we utilize an implicit s-stage diagonally implicit (DIRK) scheme with coefficients $\boldsymbol{A} \in \mathbb{R}^{s \times s}$, $\boldsymbol{b}, \boldsymbol{c} \in \mathbb{R}^s$, in the common Butcher notation, where $\boldsymbol{A} = (a_{ij})$ with $a_{ij} = 0$ for $j > i$. For the term $\Phi^*(\boldsymbol{v})$ containing the convective and reactive parts we employ an s-stage explicit scheme with coefficients $\hat{\boldsymbol{A}} \in \mathbb{R}^{s \times s}$, $\hat{\boldsymbol{b}}$, $\hat{\boldsymbol{c}} \in \mathbb{R}^s$ and $\hat{\boldsymbol{A}} = (\hat{a}_{ij})$ with $\hat{a}_{ij} = 0$ for $j \geq i$. We will denote the corresponding Butcher arrays by

$$\boldsymbol{D} := \frac{\boldsymbol{c} \mid \boldsymbol{A}}{\mid \boldsymbol{b}^{\mathrm{T}}}, \qquad \hat{\boldsymbol{D}} := \frac{\hat{\boldsymbol{c}} \mid \hat{\boldsymbol{A}}}{\mid \hat{\boldsymbol{b}}^{\mathrm{T}}}.$$

In our simulations, we limit ourselves to the second-order IMEX-RK scheme H-DIRK2(2,2,2) that corresponds to

$$\boldsymbol{D} = \frac{\begin{array}{c|cc} 1/2 & 1/2 & 0 \\ 1/2 & 0 & 1/2 \end{array}}{\begin{array}{c|cc} & 1/2 & 1/2 \end{array}}, \qquad \hat{\boldsymbol{D}} = \frac{\begin{array}{c|cc} 0 & 0 & 0 \\ 1 & 1 & 0 \end{array}}{\begin{array}{c|cc} & 1/2 & 1/2 \end{array}}.$$

Alternative choices are provided and discussed in [10, 11, 45]. If applied to the equation (1.2), the IMEX-RK scheme gives rise to the following algorithm (see [45]).

Algorithm 3.1.
    Input: *approximate solution vector $\boldsymbol{v}^n$ of* (1.2) *for $t = t^n$*
    for $p = 1, \ldots, s$
        if $p = 1$ *then*
          $\hat{\boldsymbol{v}}^{(1)} \leftarrow \boldsymbol{v}^n, \quad \bar{\boldsymbol{v}}^{(1)} \leftarrow \boldsymbol{v}^n$
        else *compute $\hat{\boldsymbol{v}}^{(p)}$ and $\bar{\boldsymbol{v}}^{(p)}$ from the known values $\boldsymbol{K}_1, \ldots, \boldsymbol{K}_{p-1}$:*
$$\hat{\boldsymbol{v}}^{(p)} \leftarrow \boldsymbol{v}^n + \Delta t \sum_{j=1}^{p-1} \hat{a}_{pj} \boldsymbol{K}_j, \quad \bar{\boldsymbol{v}}^{(p)} \leftarrow \boldsymbol{v}^n + \Delta t \sum_{j=1}^{p-1} a_{pj} \boldsymbol{K}_j$$
        endif
        solve for $\boldsymbol{K}_p$ the linear system

$$\boldsymbol{K}_p = \Phi^*\big(\hat{\boldsymbol{v}}^{(p)}\big) + \Phi\big(\bar{\boldsymbol{v}}^{(p)} + \Delta t a_{pp} \boldsymbol{K}_p\big) \tag{3.10}$$

        endfor
    $\boldsymbol{v}^{n+1} \leftarrow \boldsymbol{v}^n + \Delta t \sum_{j=1}^{s} b_j \boldsymbol{K}_j$
    Output: *approximate solution vector $\boldsymbol{v}^{n+1}$ of* (1.2) *for $t = t^{n+1} = t^n + \Delta t$.*

To solve the linear equation (3.10) that arises in Algorithm 3.1 for $\boldsymbol{K}_p$, in view of (3.9), we rewrite it as

$$\big(\boldsymbol{I} - \Delta t a_{pp} \boldsymbol{\mathcal{B}}\big) \boldsymbol{K}_p = \boldsymbol{b}^{(p)}, \quad \boldsymbol{b}^{(p)} := \Phi^*\big(\hat{\boldsymbol{v}}^{(p)}\big) + \boldsymbol{\mathcal{B}}\bar{\boldsymbol{v}}^{(p)}, \tag{3.11}$$

where $\boldsymbol{I}$ denotes the identity operator for $8 \times M \times M$ matrices. From the definition of the matrix $\boldsymbol{\mathcal{B}}$ in (3.2) and from the definition of Φ^* in (3.9), if we equate the ℓ
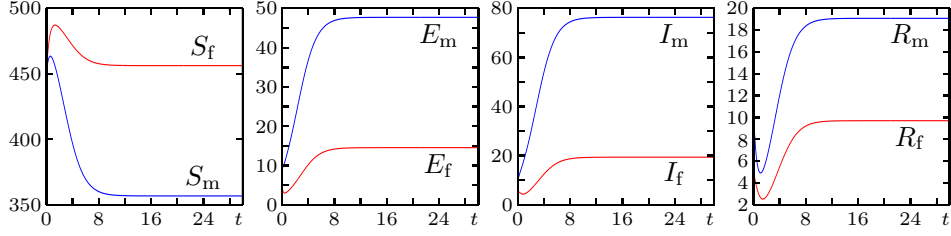
FIGURE 1. Numerical solution of the ODE version of (2.1), Model 0, for the initial data (4.1).

submatrices along the first dimension of both sides of (3.11) we get

$$
\begin{aligned}
\big(\boldsymbol{I}_{M\times M} &- \Delta t a_{pp}\mu_\ell\boldsymbol{\Delta}_h\big)(\boldsymbol{K}_p)_\ell \\
&= -\nabla_h\cdot\tilde{\boldsymbol{F}}^{\mathrm{c}}_\ell(\hat{\boldsymbol{v}}^{(p)}) + \boldsymbol{S}_\ell(\hat{\boldsymbol{v}}^{(p)}) + \mu_\ell\boldsymbol{\Delta}_h\bar{\boldsymbol{v}}^{(p)}_\ell, \quad \ell = 1,\dots,8,
\end{aligned}
\tag{3.12}
$$

where $\boldsymbol{I}_{M\times M}$ is the identity operator on $M\times M$ matrices and, e.g., $(\boldsymbol{K}_p)_\ell$ is the ℓ submatrix of $\boldsymbol{K}_p$ along the first dimension, i.e., $((\boldsymbol{K}_p)_\ell)_{i,j} = (\boldsymbol{K}_p)_{\ell,i,j}$. Some remarks are due here to detail the final implementation: for $\ell = 1,\dots,8$, the right-hand side of (3.12) is computed from (3.3), (3.2) and (3.8), taking into account that

$$
\nabla_h\cdot\tilde{\boldsymbol{F}}^{\mathrm{c}}_\ell(\hat{\boldsymbol{v}}^{(p)}) = 0 \quad \text{for } \ell \in \{5,6,7,8\}
$$

(i.e., there is no convection in the models for females); if $\mu_\ell = 0$ (for $\ell \in \{1,2,3,4\}$ and models (2.2) and (2.3) there is no diffusion term for males), then

$$
(\boldsymbol{K}_p)_\ell = -\big(\nabla_h\cdot\tilde{\boldsymbol{F}}^{\mathrm{c}}(\hat{\boldsymbol{v}}^{(p)})\big)_\ell + \boldsymbol{S}_\ell(\boldsymbol{v}),
$$

otherwise the solution of (3.12) is performed by Fast Cosine Transforms (due to boundary conditions), which entails a nearly optimal computational cost of $\mathcal{O}(M^2\log M)$.

4. Numerical examples.

4.1. **Preliminaries.** According to [4], we assume that two months (60 days) is the basic time unit, $\delta = 4$ ($1/\delta = 15\,\text{days}$), $b = 4$ (average litter size), $\beta_{\mathrm{m}} = 5\beta_{\mathrm{f}}$, and $\beta_{\mathrm{m,f}} = \beta_{\mathrm{f}}$. Moreover, the infectious period for males is assumed to be twice that of females ($1/\gamma_{\mathrm{m}} = 2/\gamma_{\mathrm{f}}$), and the carrying capacity is $K = 1000$ animals. Furthermore, we set $\beta_{\mathrm{m}} = 0.01$, $\gamma_{\mathrm{m}} = 0.5$, $a = 0.01$ and $c = 1.99\times10^{-3}$. For these values, the next-generation-matrix method [59] employed in [4] yields a basic reproductive ratio $\mathcal{R}_0 = 1.38$.

We wish to present numerical solutions of the different versions of the spatio-temporal model, Models 1 to 3, that can be compared with the example simulated in [4] (that is, by Model 0), and that corresponds to

$$
(S_{\mathrm{m}}, E_{\mathrm{m}}, I_{\mathrm{m}}, R_{\mathrm{m}}, S_{\mathrm{f}}, E_{\mathrm{f}}, I_{\mathrm{f}}, R_{\mathrm{f}})(0) = (450,10,10,10,450,5,5,5) =: \boldsymbol{U}_0^{\mathrm{T}}.
\tag{4.1}
$$

(Figure 1 shows the solution of Model 0 for this case.) To this end, we assume that the spatial domain is $\Omega = [0,1]^2$ (i.e., $L = 1$ in a scale not specified) and that $K = 1000$ is the maximum density feasible on a unit square. For the simulation, we consider Scenario 1, which corresponds to identifying a subdomain $\Omega_0 \subseteq \Omega$ with

$\Omega_0 = \{(x, y) \in \Omega : |x - 0.5| + |y - 0.5| \le 0.2\}$ in which the initial population is uniformly distributed and setting

$$\boldsymbol{u}(\boldsymbol{x}, 0) = \chi_{\Omega_0}(\boldsymbol{x})\boldsymbol{U}_0, \quad \text{where} \quad \chi_{\Omega_0}(\boldsymbol{x}) = \begin{cases} 1 & \text{if } \boldsymbol{x} \in \Omega_0, \\ 0 & \text{otherwise,} \end{cases}$$

and alternatively Scenario 2, in which we stipulate a "random" distribution by setting

$$\boldsymbol{u}(\boldsymbol{x}, 0) = \frac{1}{|\Omega|}\big(1 + r(\boldsymbol{x})\big)\boldsymbol{U}_0, \quad \text{where} \quad \int_\Omega r(\boldsymbol{x})\,\mathrm{d}\boldsymbol{x} = 0 \qquad (4.2)$$

and r is a given oscillatory function assuming values in $(-1, 1)$. (The idea is not to impose any initial "pattern" in Scenario 2.)

A total number of six cases is considered by combining Scenarios 1 and 2 with Models 1, 2 and 3. We always choose $\mu_X = 0.05$ for all species X, $\kappa_X = 0.1$ and $h = 1/200$. Furthermore, we wish to compare the numerical results with the predictions made by the non-spatial ODE model, Model 0 (Figure 1). To this end we determine for each compartment $X \in \mathcal{C}$ and time instants $t^n = n\Delta t$ the following quantity:

$$\mathcal{I}(X) = \mathcal{I}(X, t^n) := h^2 \sum_{i,j=1}^{\mathrm{N}} X_{i,j}^n \approx \int_\Omega X(\boldsymbol{x}, t^n)\,\mathrm{d}\boldsymbol{x}, \qquad (4.3)$$

which represents the approximate total number in Ω of individuals of compartment X at time t^n. We recall that in the PDE model (2.1), the unknowns $X \in \mathcal{C}$ are *densities*, and so an integration over Ω is necessary to make results comparable to those of a model that predicts the *total number* of individuals in each compartment (as does Model 0). Similar "integrals" of the numerical solution are utilized by Colombo and Rossi [20, Fig. 3.2] to study the global behaviour of their predator-prey model.

4.2. **Cases 1 to 3: simulations with a structured initial datum.** In Figures 2 to 4 we show the numerical solution for N_m, N_f, I_m and I_f, in each case at three different times, for Cases 1 to 3 that arise for Scenario 1 with Model 1, Model 2 with $K = 1000$, and Model 3. First of all, we observe that according to the results for N_m and I_m, within Models 1 and 2 the male individuals keep confined to a growing but sharply limited region, with zero values outside that region. Model 3, with its linear diffusive term $-\mu_X \nabla X$ for $X \in \mathcal{C}_\mathrm{m}$ (instead of the expressions $-\mu_X X \boldsymbol{V}(N_\mathrm{m})$ or $-\mu_X X \varphi(N_\mathrm{m} + N_\mathrm{f})\boldsymbol{V}(N_\mathrm{m})$ in Models 1 or 2), produces a solution that fills the entire domain. Numerical results obtained for larger times than those shown in Figure 4 indicate that the solutions of all variables become constant on the entire computational domain, and the integral quantities assume a stationary state similar (but not identical) to that of Model 0 (see Figure 1). Furthermore, comparing the results between Models 1 and Models 2 (Figures 2 and 3), we observe that Model 1 gives rise to a distinct spatial structure, including regions that are nearly void of males combined with "peaks" of the solution where $N_\mathrm{m} \approx 1500$. Clearly, this feature is expected since Model 1 has no mechanism that would limit the value of the total density of males N_m. (We recall that although the total numbers of male or female individuals, $\mathcal{I}(N_\mathrm{m})$ and $\mathcal{I}(N_\mathrm{f})$, are bounded by the terms with the death rates in all models, it may well happen that the densities N_m or N_f become locally unbounded.)

The results obtained for Case 1 are in marked contrast to those for Case 2, especially those for N_m, produced by Model 2 shown in Figure 3, where we observe
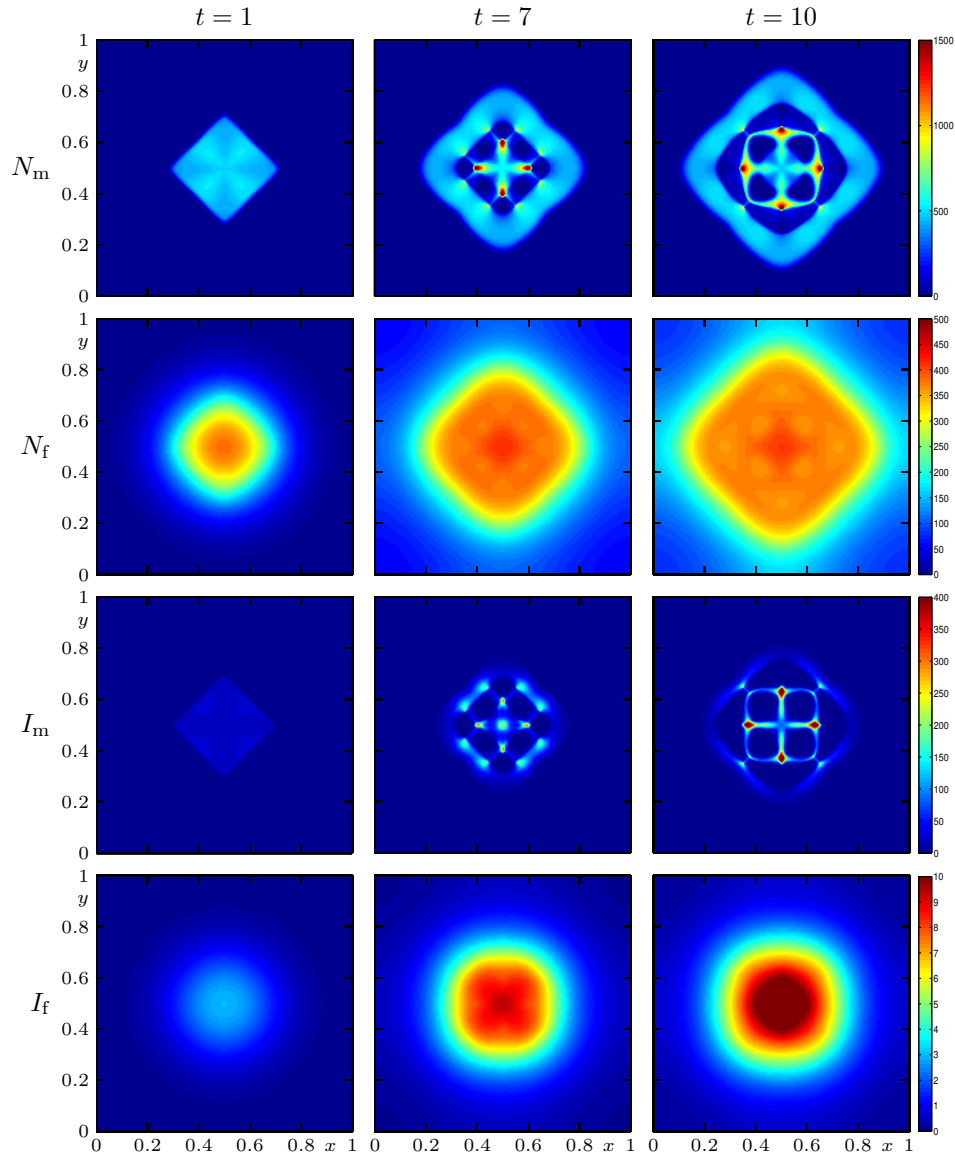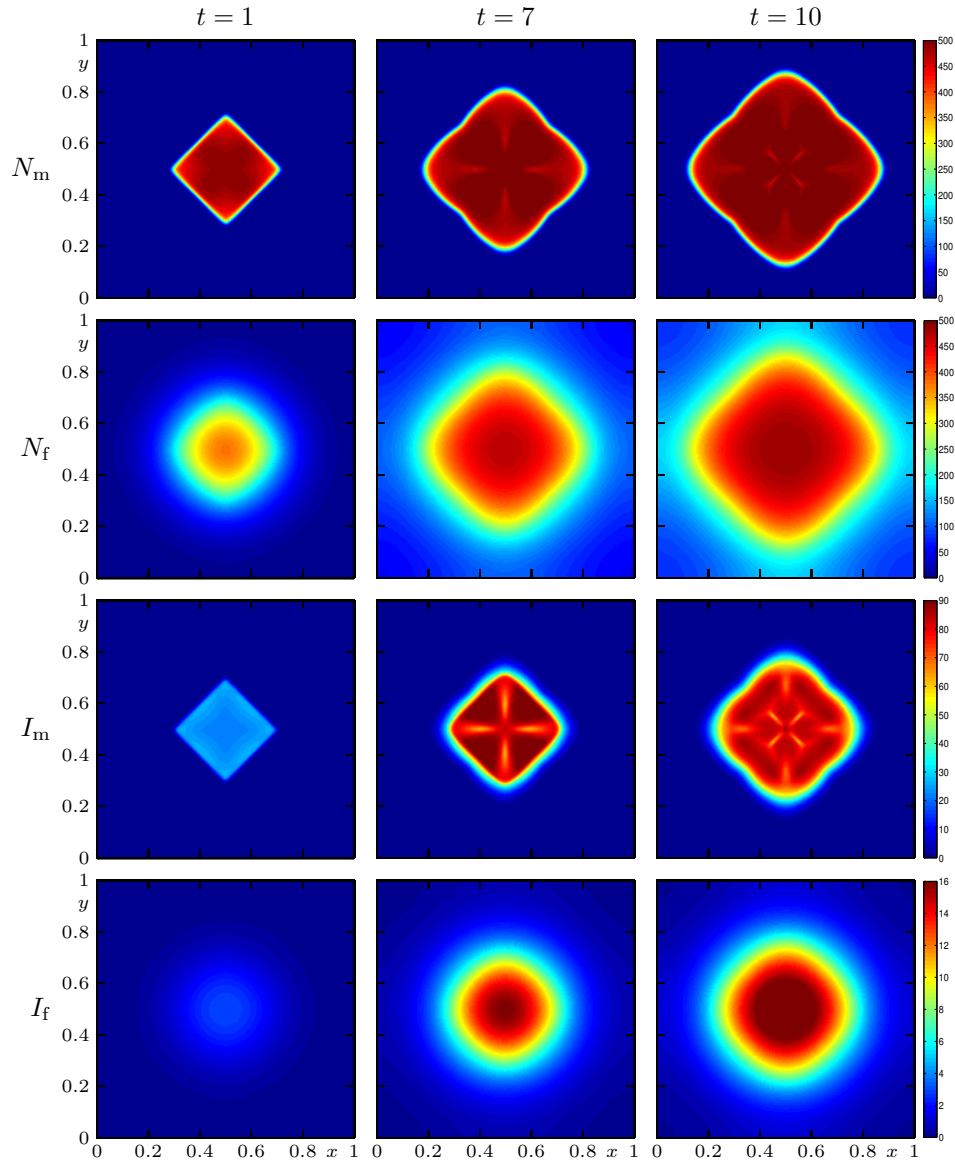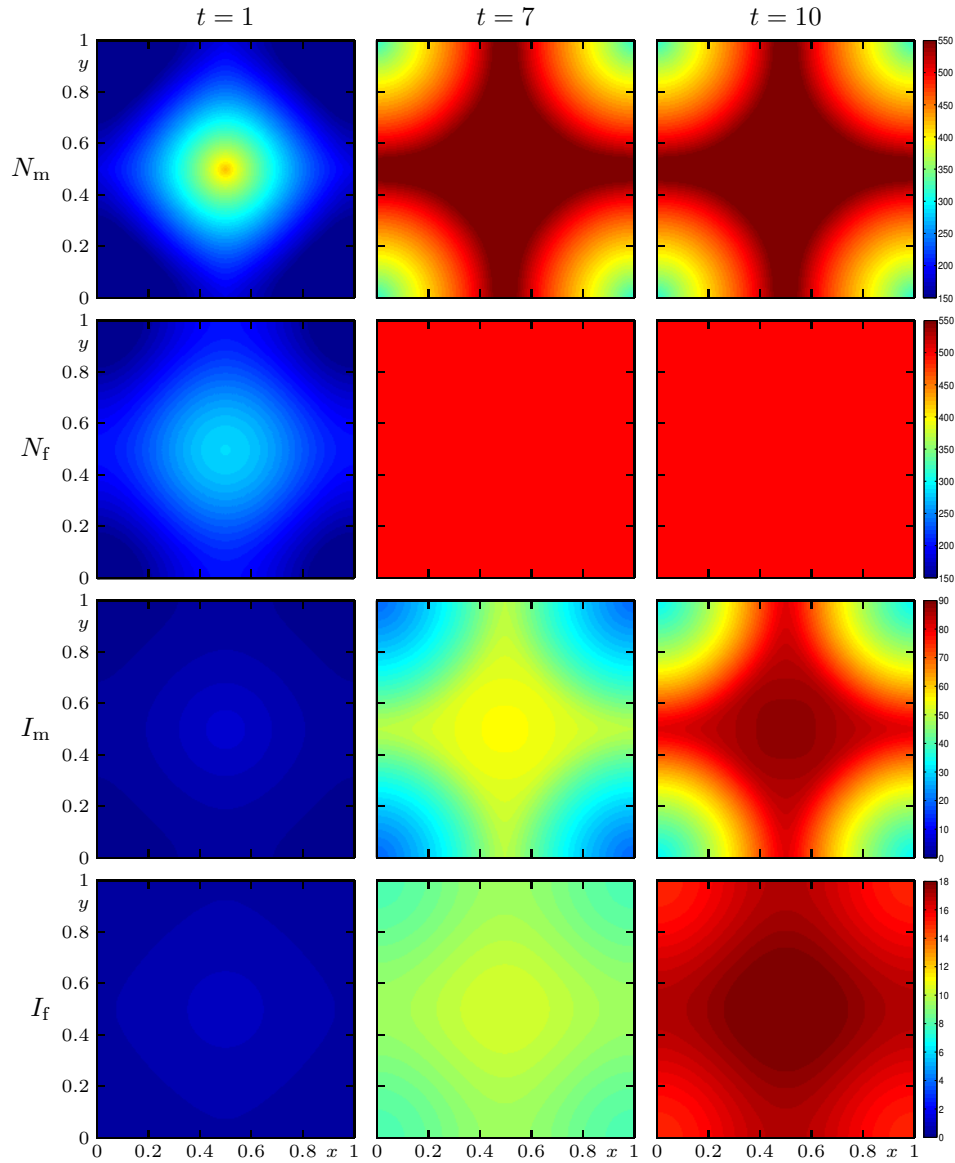
FIGURE 2. Case 1 (Model 1, Scenario 1): numerical solution for N_m, N_f, I_m and I_f at the indicated times.

that N_m does not exceed a value of about 500, and stays close to that value within a region of approximately the same shape as for Model 1. A similar observation is true for the compartment I_m: Model 1 (Figure 2) predicts a structure with "peaks" that roughly mirrors that of N_m, while Model 2 (Figure 3¿) predicts a more uniform distribution (with I_m assuming values between 70 and 90) in the interior of the domain. Furthermore, we recall that for all models the flux for the female compartments is always given by $-\mu_X \nabla X$ for $X \in \mathcal{C}_f$, so differences in solution behavior of the female individuals are exclusively due to those in describing

FIGURE 3. Case 2 (Model 2 with $K = 1000$, Scenario 1): numerical solution for N_m, N_f, I_m and I_f at the indicated times.

the male behavior. In general, this diffusive behavior tends to produce less sharp, smooth spatial structures.

Finally, Figure 5 indicates that Models 1, 2 and 3 lead to quite different numerical results in terms of the integrated quantities (4.3). As mentioned above, the results of Model 3 are similar to those of Model 0. On the other hand, while Models 1 and 2 produce integral results whose order of magnitude for each compartment is similar to that of Model 3, it can be noted that no stationary state is attained at $t = 30$; as the discussion of Cases 4 to 6, and in particular comparing Figures 5 and 9 show,

FIGURE 4. Case 3 (Model 3, Scenario 1): numerical solution for
N_m, N_f, I_m and I_f at the indicated times.

this is a consequence of the respective model structure in combination with the
choice of initial data. In any case, it is calling to attention that while Models 2
and 3 predict a smooth variation of the integrated quantity in time, the curves
generated by Model 1 are somewhat oscillatory. This behavior is consistent with
our observation that Model 1 does not only generate a spatial solution structure with
strong variations, "peaks" and sharp gradients, but also produces rapid transitions
within time. This unsteady and unstable behavior is due to the strong competence
of advective and repulsive mechanisms inherent in the definition (2.2).
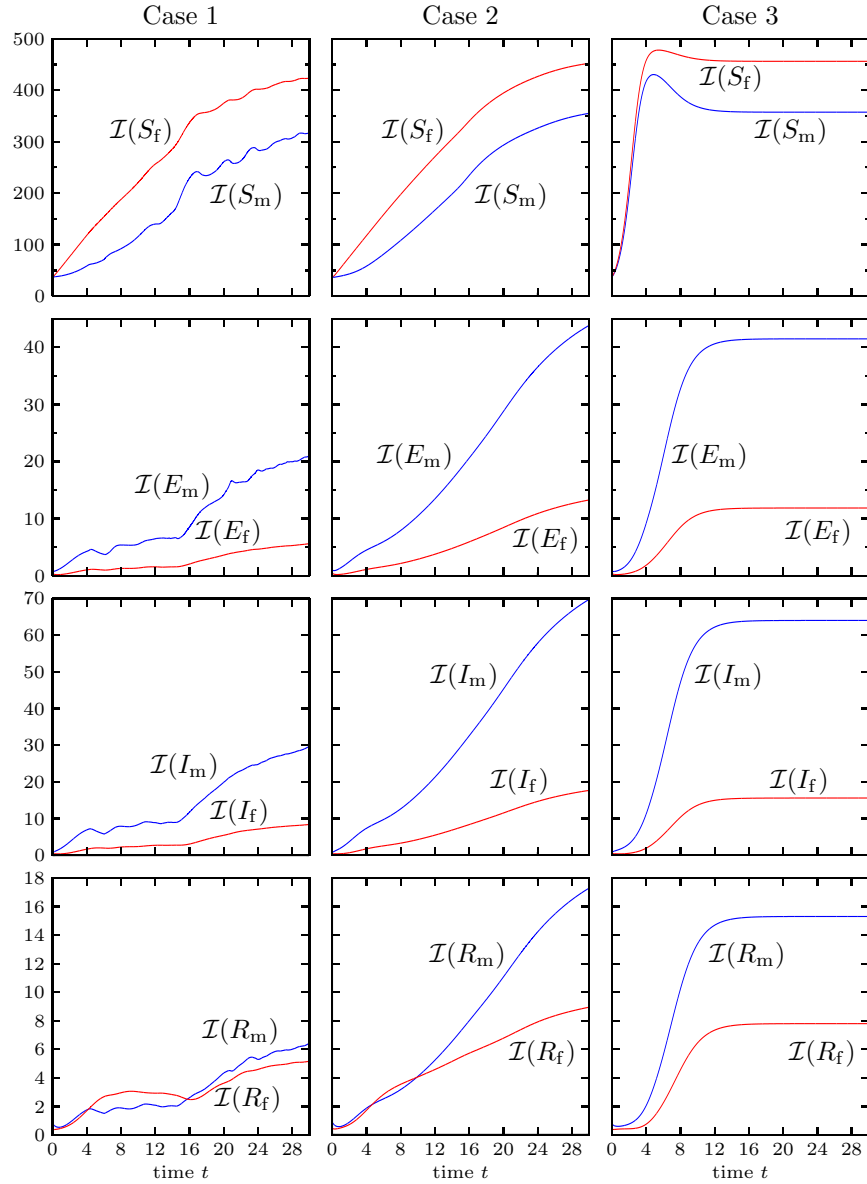
FIGURE 5. Cases 1–3: integral quantities $\mathcal{I}(X)$ defined by (4.3) for each compartment obtained by evaluating numerical solutions.

4.3. **Cases 4 to 6: simulations with a randomly fluctuating initial datum.** Figures 6 to 9 provide numerical solutions for Scenario 2. The "random" initial datum (4.2) has been chosen to test whether small perturbations would give rise to large-scale regular structures akin to the well-known mechanism of pattern formation (cf., e.g., [38, 41]), or rather, the small fluctuations in the initial datum would simply be smoothed out. Figure 6, corresponding to Model 1, illustrates that male individuals aggregate in a kind of filamentous structure, including some marked peaks with N_m reaching values close to 3000. On the other hand, we observe the
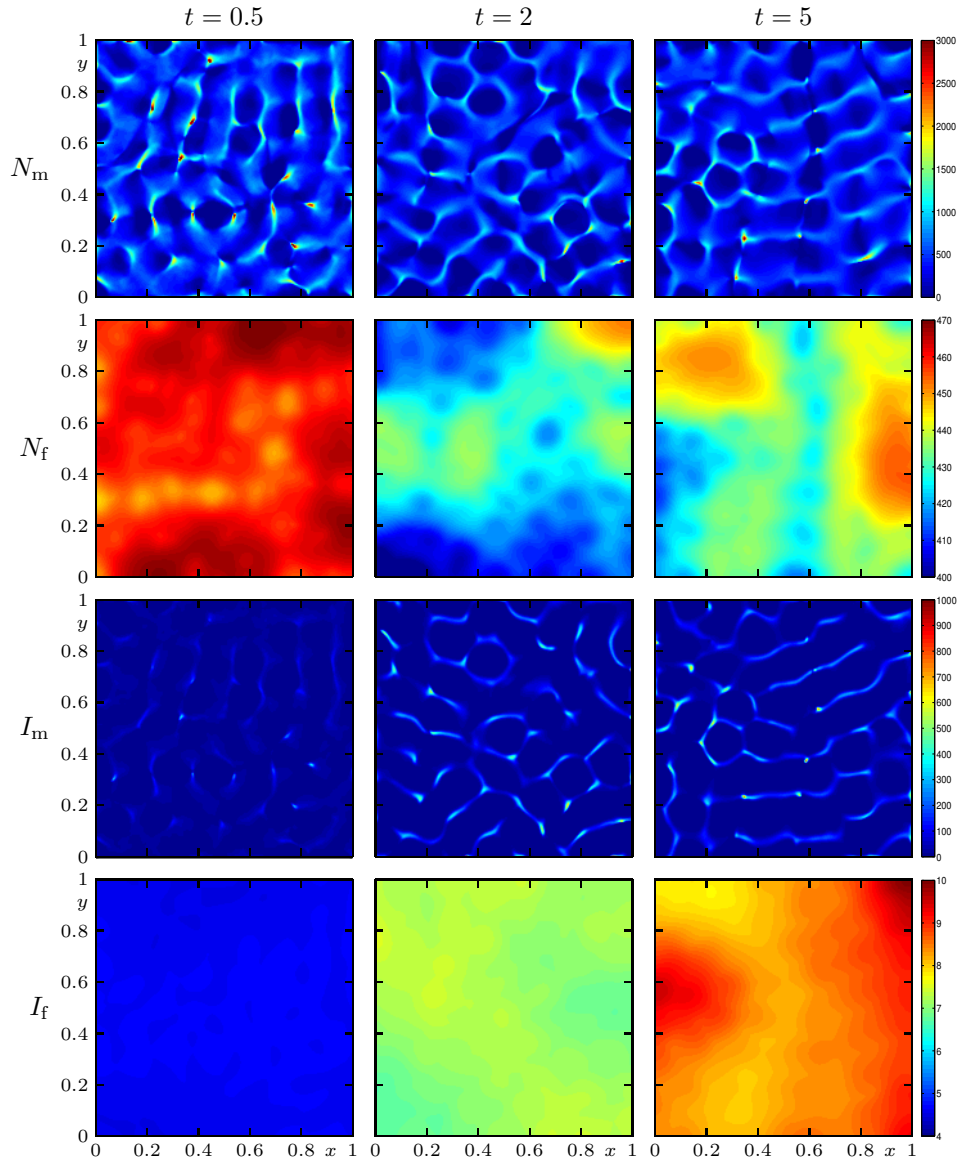
FIGURE 6. Case 4 (Model 1, Scenario 2): numerical solution for N_{m}, N_{f}, I_{m} and I_{f} at the indicated times.

formation of areas of roughly the same shape and size that are nearly void of male individuals. This behavior is similar to that observed by Colombo and Rossi for the predator density in their predator-prey model (cf., e.g., [20, Figs. 3.3–3.5]). In our cases, the densities of the female populations N_{f} and I_{f} do not vary much over the computational domain, and do so smoothly. For the same scenario with Model 2 and $K = 1000$, Figure 7 indicates that while for small times we observe the formation of spatial structures similar those of Figure 6, eventually all variables become nearly constant on the whole domain. Figure 8 for Model 3 illustrates that marked
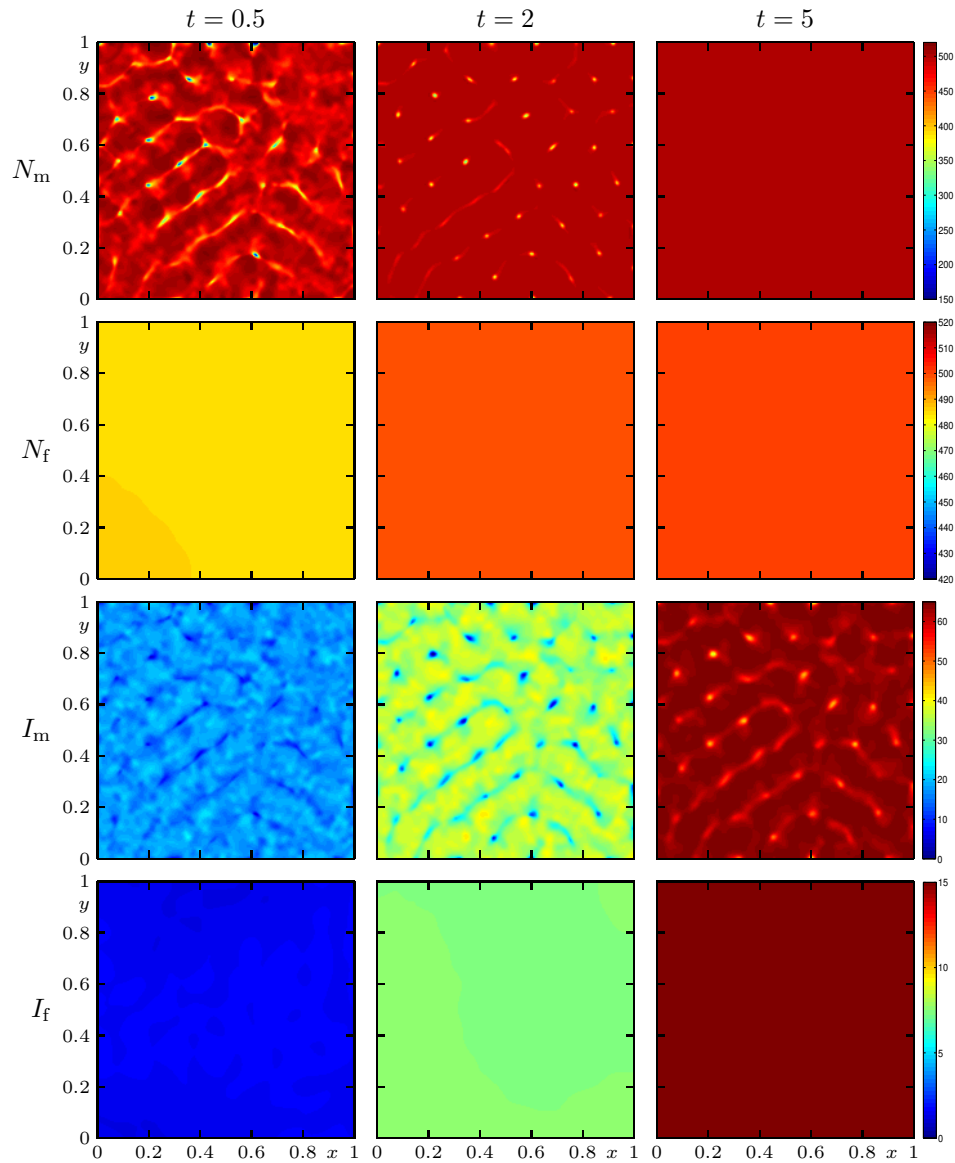
FIGURE 7. Case 5 (Model 2 with $K = 1000$, Scenario 2): numerical solution for N_m, N_f, I_m and I_f at the indicated times.

circular spatial structures persist over long times. Similar results (not shown here) were obtained in other numerical experiments for times up to $t = 87$. We also comment that Figure 9 illustrates that Model 2 leads to a nearly stationary behavior of the integral quantities within shorter time than for Scenario 1, and results for Models 2 and 3 are quite similar. The curves observed in Figure 9 for Model 1 are, again, oscillatory, which lends further support to the conjecture that this model (at least with the parameters chosen) exhibits spatial-temporal oscillatory behavior.
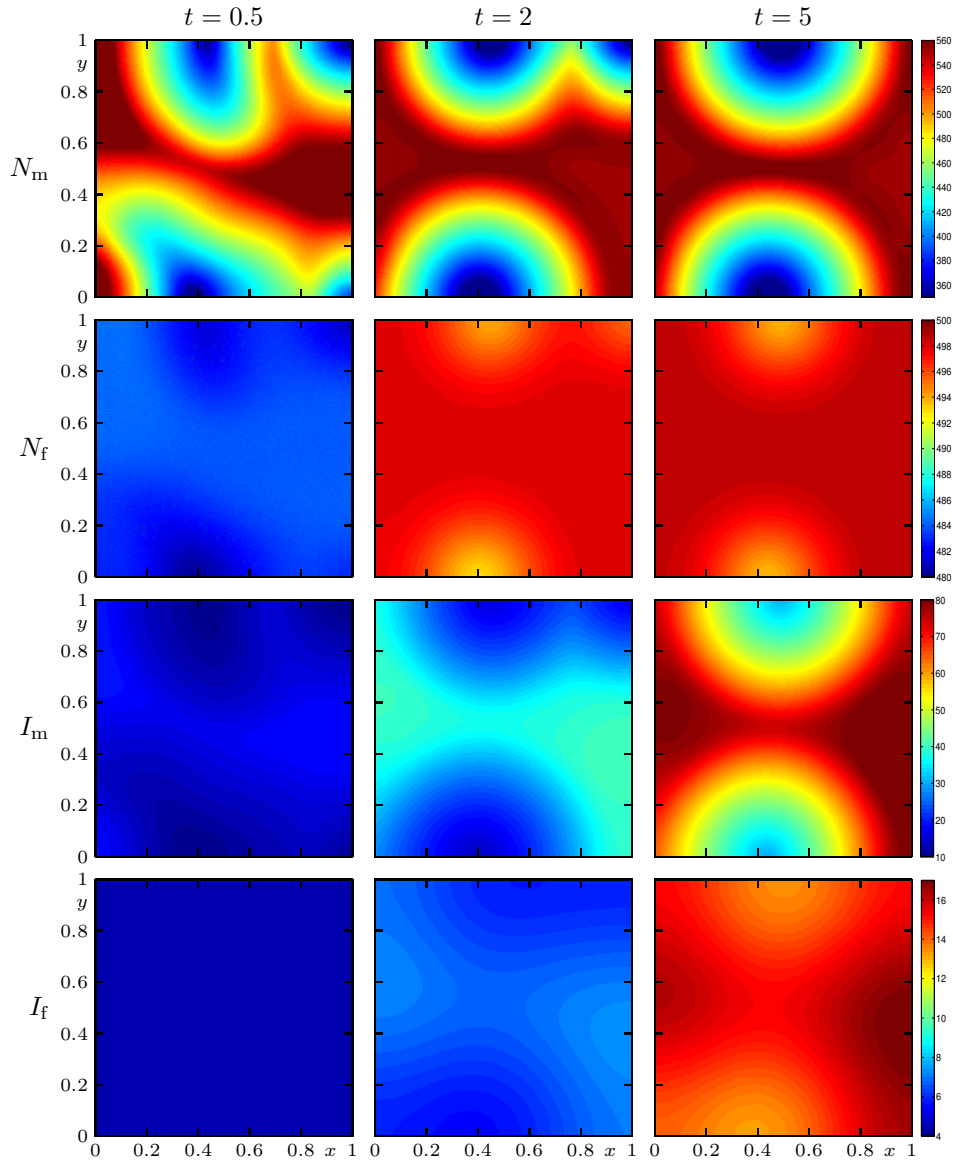
FIGURE 8. Case 6 (Model 3, Scenario 2): numerical solution for N_{m}, N_{f}, I_{m} and I_{f} at the indicated times.

For Cases 4 to 6, we calculate the evolution of Moran's index [25,40,49], denoted here I, for each species at each time step, and which is here computed by

$$\mathsf{I} = \mathsf{I}(X) := \sum_{i,j=1}^{M} \frac{1}{4} Y_{i,j} \big(Y_{i-1,j} + Y_{i+1,j} + Y_{i,j-1} + Y_{i,j+1} \big) \bigg/ \sum_{i,j=1}^{M} Y_{i,j}^2, \qquad (4.4)$$
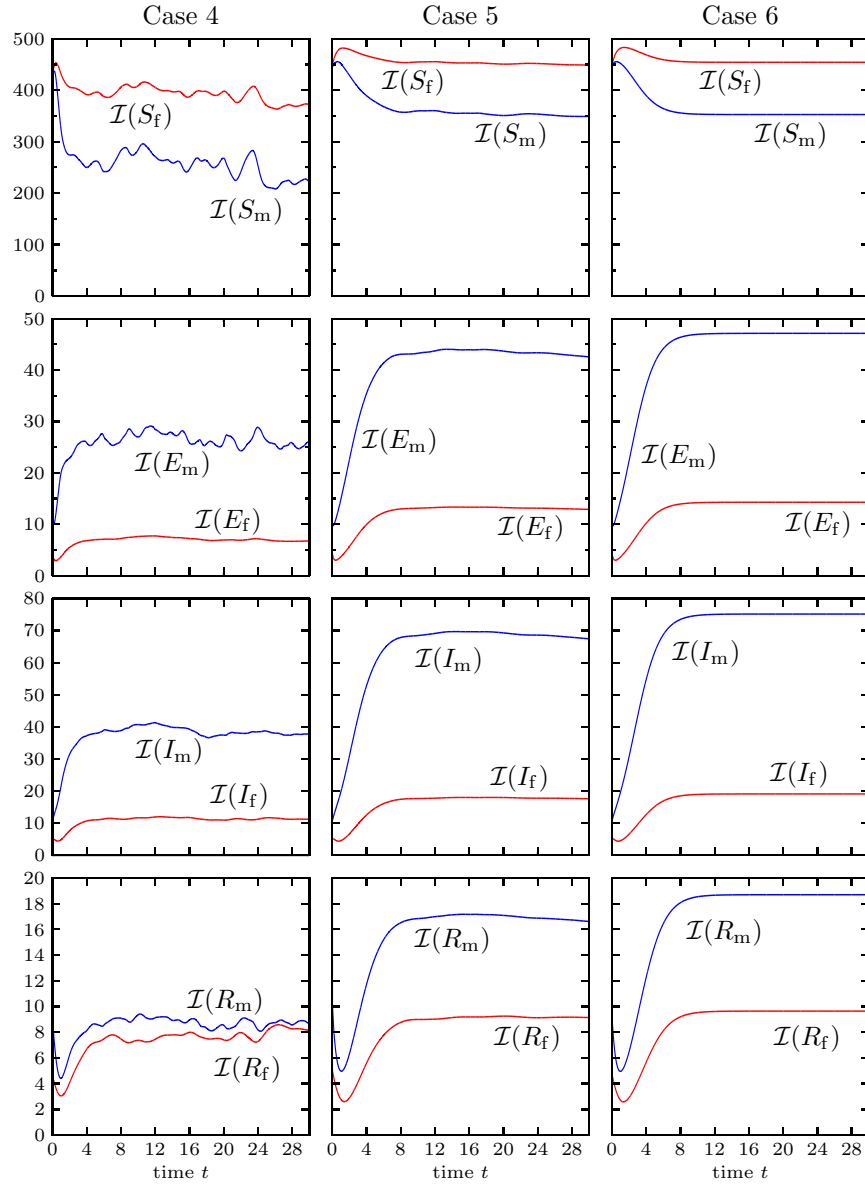
FIGURE 9. Cases 4–6: integral quantities $\mathcal{I}(X)$ defined by (4.3) for each compartment obtained by evaluating numerical solutions.

where X is the numerical data obtained for some species at a certain time step and

$$Y_{i,j} = X_{i,j} - \frac{1}{M^2} \sum_{p,q=1}^{M} X_{p,q}. \tag{4.5}$$

Overall, the results shown in Figure 10 indicate that a strong spatial autocorrelation ($I \approx 1$) is developed through the simulation from initial random data ($I \approx 0$). It is, however, interesting to note for that for Cases 4 and 5 the values of I for the
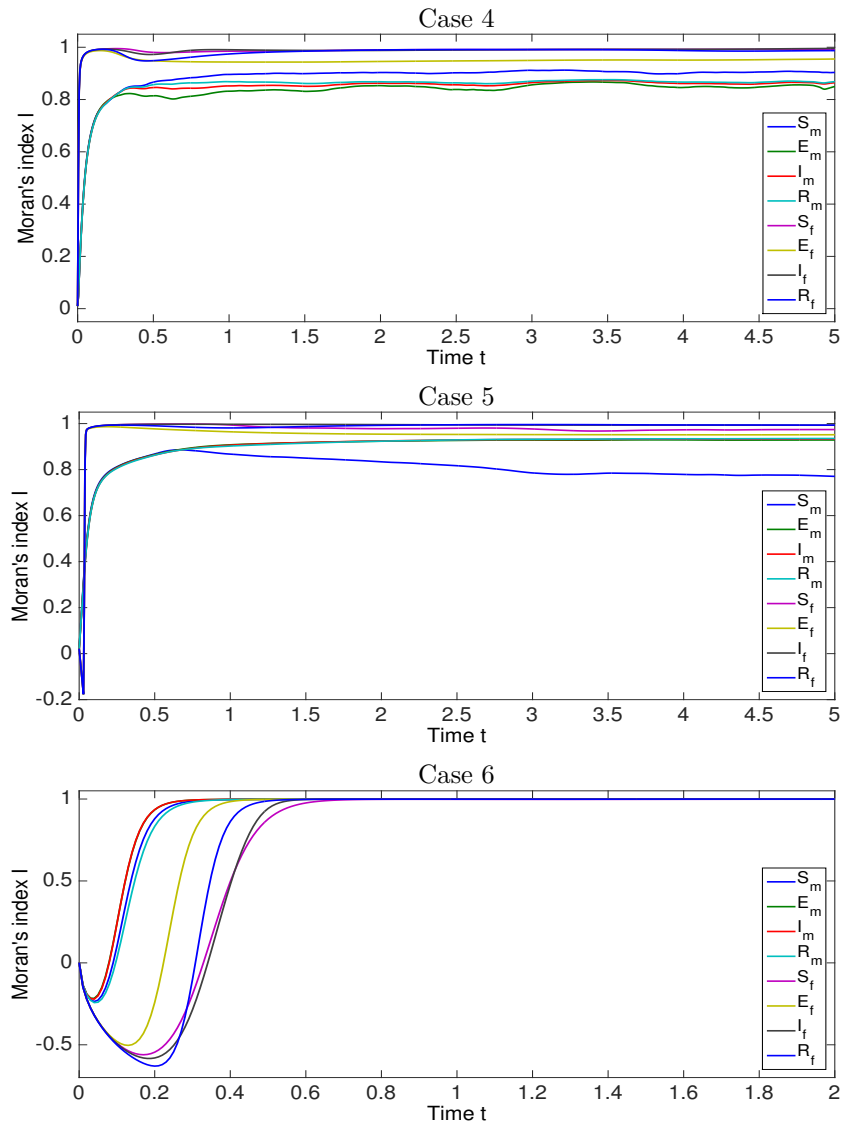
FIGURE 10. Cases 4–6: Moran's index I defined by (4.4), (4.5) for each compartment obtained by evaluating numerical solutions.

female compartments remain consistently below those of the male compartments, while for Case 6 the limit value I = 1 is closely approximated by all species. This confirms the trend evident already from the results of Figure 8 compared with those of Figures 6 and 7, namely that the presence of diffusive movement in the male species significantly contributes to generating smoothly varying solution patterns, that is, to creating a high degree of spatial autocorrelation.

4.4. **Case 7: order test with smooth solution.** The purpose of this test is to show that the numerical scheme exhibits experimental second order convergence
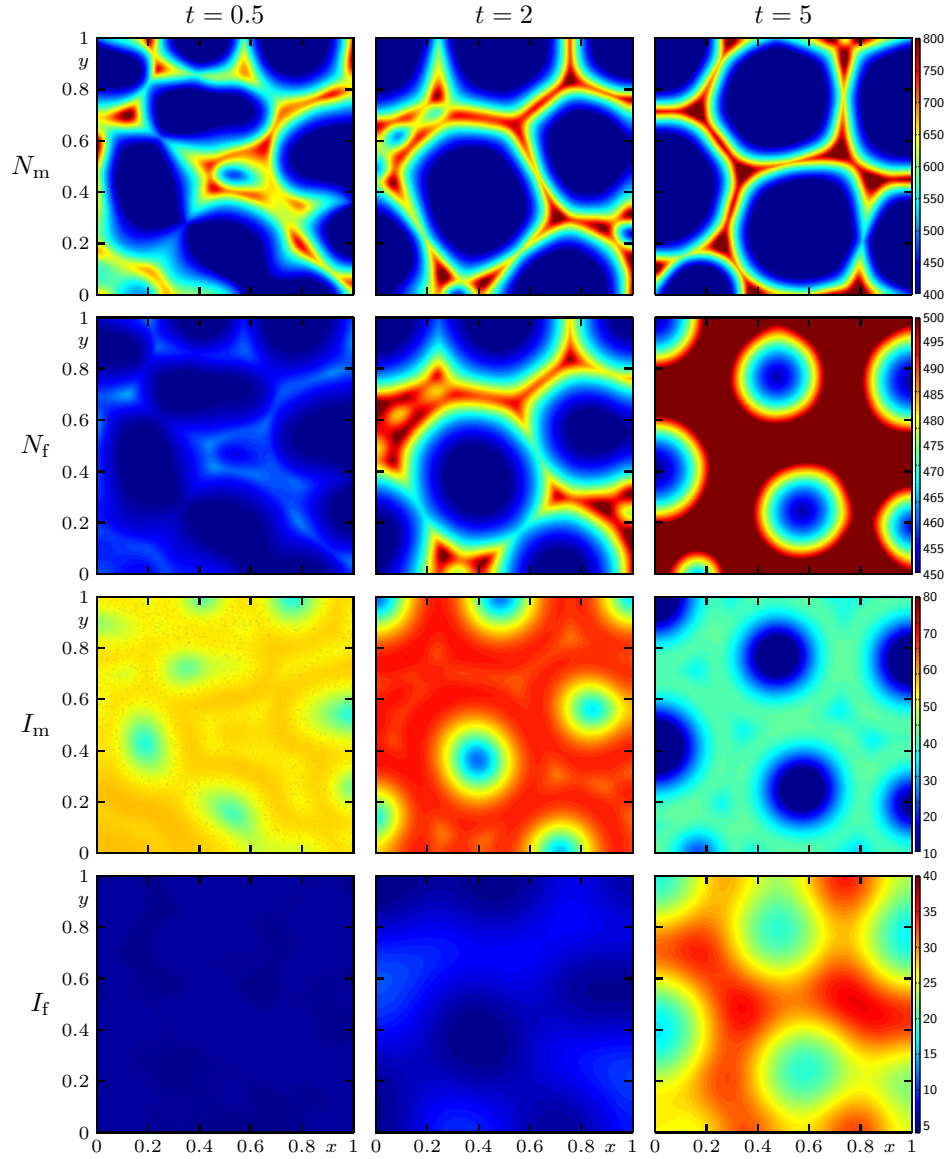
FIGURE 11. Case 8 (Model 3, Scenario 2, periodic variation of parameters): numerical solution for N_{m}, N_{f}, I_{m} and I_{f} at the indicated times.

when the solution is smooth. For this purpose, we choose a smooth initial configuration given by

$$X_{\mathrm{m}}(x, y, t = 0) = c_X \exp\left(-\frac{1}{2}\left((x-3)^6 + (y-3)^6\right)\right),$$

$$X_{\mathrm{f}}(x, y, t = 0) = c_X \exp\left(-\frac{1}{2}\left((x-7)^6 + (y-7)^6\right)\right)$$
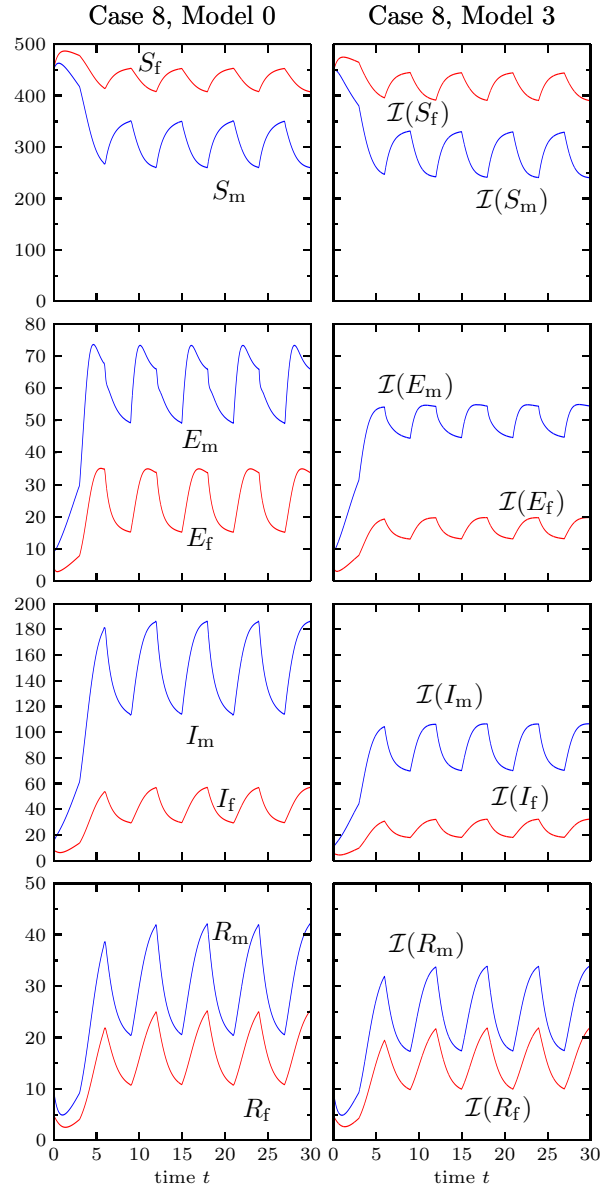
FIGURE 12. Case 8: (Model 3, Scenario 2, periodic variation of parameters): solutions of Model 0 (left column) and integral quantities $\mathcal{I}(X)$ of Model 3 (right column) defined by (4.3) for each compartment obtained by evaluating numerical solutions.

for $X \in \{S, E, I, R\}$, constants $c_S = 1000$, $c_E = 1$, $c_I = 10$ and $c_R = 1$, and a sufficiently small final time $T = 0.1$ to ensure that no singularities are formed during the simulation. We choose $\mu_X = 10^{-4}$ for $X \in \mathcal{C}_m$ and $\mu_X = 10^{-3}$ and $\kappa_X = 10^{-2}$ for $X \in \mathcal{C}_f$.

M	8	16	32	64	128	256
$e_M^{tot} \times 10^3$	368.90	383.19	379.01	153.73	34.70	9.14
θ_M	-0.05	0.02	1.30	2.15	1.92	—

TABLE 1. Case 7 (Model 1, order test with smooth solution): approximate total L^1 errors e_M^{tot} and observed convergence rates θ_M.

We compute approximate L^1 errors for approximate solutions obtained with $M \times M$ meshes, $M = 2^s$, $s = 3, \ldots, 8$, using a reference solution with a resolution of $M_{\text{ref}} \times M_{\text{ref}}$ cells, for $M_{\text{ref}} = 2048$, as follows. We denote by $(v_{\ell,j,k}^M)_{j,k=1}^M$ and $(v_{\ell,j,k}^{\text{ref}})_{j,k=1}^{M_{\text{ref}}}$ the numerical solution for the ℓ-th component ($\ell = 1, \ldots, 8$, see Section 3.3) at time T calculated with M and M_{ref}, respectively. We project the reference solution to the coarser grids by bicubic interpolation, since the numerical scheme is designed to compute second-order approximations to the exact solutions at the nodes (x_i, y_j), with $x_i = y_i = (i-1/2)L/M$, for the coarse mesh, and $(\bar{x}_i, \bar{y}_j)$, with $\bar{x}_i = \bar{y}_i = (i-1/2)L/M_{\text{ref}}$ for the fine mesh and these points do not coincide. Specifically, this projection $\tilde{v}_{\ell,j,k}^M$ for $j, k = 1, \ldots, M$ is computed by

$$\tilde{v}_{\ell,j,k}^M = \sum_{j_1,k_1=-2}^{1} \xi_{j_1}\xi_{k_1} v_{\ell,\bar{j}-j_1,\bar{k}-k_1}^{\text{ref}}, \quad \bar{j} = \left(j - \frac{1}{2}\right)\frac{M_{\text{ref}}}{M}, \quad \bar{k} = \left(k - \frac{1}{2}\right)\frac{M_{\text{ref}}}{M},$$

where $\xi_{-2} = \xi_1 = -1/16$ and $\xi_0 = \xi_{-1} = 9/16$. Notice that $M_{\text{ref}}/M = 2^{11-s} \geq 8$ in this test and the previous formula is therefore computable.

The total approximate L^1 error of the numerical solution $(v_{\ell,j,k}^M)_{j=1}^M$ at time T is then given by

$$e_M^{\text{tot}} := \frac{1}{M^2} \sum_{\ell=1}^{8} \sum_{j,k=1}^{M} \left| \tilde{v}_{\ell,j,k}^M - v_{\ell,j,k}^M \right|. \tag{4.6}$$

Based on the approximate errors defined by (4.6), we may calculate a numerical order of convergence from pairs of total approximate L^1 errors e_M^{tot} and e_{2M}^{tot} by

$$\theta_M := \log_2\left(e_M^{\text{tot}}/e_{2M}^{\text{tot}}\right).$$

These data are displayed in Table 1. It can be deduced that the errors start diminishing for $M = 64$ and do so roughly at a second-order rate.

4.5. **Case 8: seasonal alternation for Models 0 and 3.** Climatic changes, e.g., due to large periods of rain or of drought, can lead to variation in some parameters, for example those that influence death and birth rates of the rodent population. To study the effect of seasonal variability, in this example we identify two different sets of parameters that can represent two different seasons, $\{a_i, b_i, c_i\}$ for $i = 1, 2$. We wish to explore the transmission dynamics of hantavirus due to an alternation in time of the parameters between these two seasons. We implement square-periodic season alternation where the duration of each season is $T/2$, where T units is a year. Any given quantity $u(t)$ alternating in this way can be expressed as $u(t) = u_+ + u_-\mu(t)$, where $u_\pm = \frac{1}{2}(u_1 \pm u_2)$ and $\mu(t)$ is a periodic square wave $\mu(t) = 1$ if $t \in (0, T/2)$ and $\mu(t) = -1$ if $t \in (T/2, T)$.

We consider $a_1 = 0.01$, $b_1 = 4$, $c_1 = 1.99 \times 10^{-3}$ and $a_2 = 0.05$, $b_2 = 3$, $c_2 = 0.0015$ in order for the carrying capacity to be $K_1 = K_2 = 1000$ for both choices, so $R_{0,1} = 1.38$ and $R_{0,2} = 2.26$ are obtained. The remaining parameters and initial conditions are the same as in Cases 4 to 6 (Scenario 2).

In Figure 11 we display the numerical solution for Model 3. Roughly speaking we observe that the seasonal alternation in the parameters produces a solution similar to that provided by Model 3 also with a randomly fluctuating initial datum. In Figure 12 we display the solutions for (the ODE) Model 0 and for Model 3. We observe that the seasonal alternation in the parameters generates an oscillatory and bounded solution for each case, and Model 3 displays a smaller amplitude.

5. **Conclusions.** We have shown that a relatively simple gender-structured spatial-temporal model (2.1) of Hantavirus transmission among rodents with a non-local velocity term (2.6), which arises in each of the Models 1, 2 and 3 defined by (2.2), (2.3) and (2.5), respectively, can yield complex spatial-temporal profiles of disease prevalence (Figures 2 to 8). However, in reality, a number of additional factors can affect the transmission dynamics of Hantavirus infections among rodents. Specifically, the transmission of hantavirus has been associated with land use patterns, elevation, vegetation types [9], as well as variations in temperature, humidity, and rainfall [64]. Moreover, rodent habitat and rodent behavior can be influenced by temperature, precipitation and land use [16]. The growth of rodent populations may also be associated with local temperature, as temperature may affect the pregnancy rate, litter size, birth rate and the survival rate of rodent populations [62]. Further, rodents tend to inhabit highly covered and less disturbed habitats, which are commonly found in agricultural habitats and pastureland habitats [39, 63] in order to enhance their reproduction and survival capacity [39].

We plan to conduct further research on the qualitative analysis of the proposed models, or suitable simplifications of them, using analogous techniques to those utilized in [20]. The accuracy of the numerical method proposed in this work is worth to be studied in subsequent works, specially to establish that its order of convergence corresponds to its design order. Although in this work we use a second-order spatial discretization of the Laplacian and a second-order time-stepping, which limit the high-order accuracy of the fifth-order WENO spatial semidiscretization, we plan to perform comparisons with higher-order discretizations of the diffusion operator and time-stepping scheme. More scenarios (initial configuration, parameter calibration) should be explored with these numerical tools in order to obtain and study further spatio-temporal patterns in the simulations. In this sense, among our proposed models, we consider that Model 1 is the most promising one giving rise to interesting spatio-temporal patterns and is worth to be analyzed as in [19, 38]. Finally, we wish to expand on the conclusions that can be inferred from I applied to numerical solutions of a local or non-local PDEs, which to our knowledge still needs to be addressed. We leave an in-depth analysis of the behaviour of I and related quantities, such as the bivariate Moran index [25, 49] that could, for example, elucidate the mutual spatial correlation of the male and female patterns, as a topic of future research for the present class of models.

REFERENCES

[1] G. Abramson and V. M. Kenkre, Spatiotemporal patterns in the Hantavirus infection, *Phys. Rev. E*, **66** (2002), 011912 (5pp).

[2] M. A. Aguirre, G. Abramson, A. R. Bishop and V. M. Kenkre, Simulations in the mathematical modeling of the spread of the Hantavirus, *Phys. Rev. E*, **66** (2002), 041908 (5pp).

[3] L. J. S. Allen, B. M. Bolker, Y. Lou and A. L. Nevai, Asymptotic of the steady states for an SIS epidemic patch model, *SIAM J. Appl. Math.*, **67** (2007), 1283–1309.

[4] L. J. S. Allen, R. K. McCormack and C. B. Jonsson, Mathematical models for hantavirus infection in rodents, *Bull. Math. Biol.* **68** (2006), 511–524.

[5] R. M. Anderson and R. M. May, *Infectious Diseases of Humans: Dynamics and Control*, Oxford Science Publications, 1991.

[6] J. Arino, Diseases in metapopulations. In *Z. Ma, Y. Zhou and J. Wu (Eds.), Modeling and Dynamics of Infectious Diseases,* Higher Education Press, Beijing, **11** (2009), 64–122.

[7] J. Arino, J. R. Davis, D. Hartley, R. Jordan, J. M. Miller and P. van den Driessche, A multi-species epidemic model with spatial dynamics, *Mathematical Medicine and Biology*, **22** (2005), 129–142.

[8] U. Ascher, S. Ruuth and J. Spiteri, Implicit-explicit Runge-Kutta methods for time dependent partial differential equations, *Appl. Numer. Math.*, **25** (1997), 151–167.

[9] P. Bi, X. Wu, F. Zhang, K. A. Parton and S. Tong, Seasonal rainfall variability, the incidence of hemorrhagic fever with renal syndrome, and prediction of the disease in low-lying areas of China, *Amer. J. Epidemiol.*, **148** (1998), 276–281.

[10] S. Boscarino, R. Bürger, P. Mulet, G. Russo and L. M. Villada, Linearly implicit IMEX Runge-Kutta methods for a class of degenerate convection-diffusion problems, *SIAM J. Sci. Comput.*, **37** (2015), B305–B331.

[11] S. Boscarino, F. Filbet and G. Russo, High order semi-implicit schemes for time dependent partial differential equations, *J. Sci. Comput.* **68** (2016), 975–1001.

[12] S. Boscarino, P. G. LeFloch and G. Russo, High-order asymptotic-preserving methods for fully nonlinear relaxation problems, *SIAM J. Sci. Comput.*, **36** (2014), A377–A395.

[13] S. Boscarino and G. Russo, On a class of uniformly accurate IMEX Runge-Kutta schemes and applications to hyperbolic systems with relaxation, *SIAM J. Sci. Comput.*, **31** (2009), 1926–1945.

[14] S. Boscarino and G. Russo, Flux-explicit IMEX Runge-Kutta schemes for hyperbolic to parabolic relaxation problems, *SIAM J. Numer. Anal.*, **51** (2013), 163–190.

[15] F. Brauer and C. Castillo-Chavez, *Mathematical Models in Population Biology and Epidemiology*, Second Ed., Springer, New York, 2012.

[16] M. Brummer-Korvenkontio, A. Vaheri, T. Hovi, C. H. von Bonsdorff, J. Vuorimies, T. Manni, K. Penttinen, N. Oker-Blom and J. Lähdevirta, Nephropathia epidemica: Detection of antigen in bank voles and serologic diagnosis of human infection. *J. Infect. Dis.*, **141** (1980), 131–134.

[17] J. Buceta, C. Escudero, F. J. de la Rubia and K. Lindenberg, Outbreaks of Hantavirus induced by seasonality, *Phys. Rev. E*, **69** (2004), 021908 (9pp).

[18] R. Bürger, G. Chowell, P. Mulet and L. M. Villada, Modelling the spatial-temporal progression of the 2009 A/H1N1 influenza pandemic in Chile, *Math. Biosci. Eng.*, **13** (2016), 43–65.

[19] R. Bürger, R. Ruiz-Baier and C. Tian, Stability analysis and finite volume element discretization for delay-driven spatio-temporal patterns in a predator-prey model, *Math. Comput. Simulation*, **132** (2017), 28–52.

[20] R. M. Colombo and E. Rossi, Hyperbolic predators versus parabolic preys, *Commun. Math. Sci.*, **13** (2015), 369–400.

[21] M. Crouzeix, Une méthode multipas implicite-explicite pour l'approximation des équations d'évolution paraboliques, *Numer. Math.*, **35 (1980)**, 257–276.

[22] O. Diekmann, H. Heesterbeek and T. Britton, *Mathematical Tools for Understanding Infectious Disease Dynamics*, Princeton Series in Theoretical and Computational Biology, Princeton University Press, Princeton, NJ, 2013.

[23] R. Donat and I. Higueras, On stability issues for IMEX schemes applied to 1D scalar hyperbolic equations with stiff reaction terms, *Math. Comp.*, **80** (2011), 2097–2126.

[24] C. Escudero, J. Buceta, F. J. de la Rubia and K. Lindenberg, Effects of internal fluctuations on the spreading of Hantavirus, *Phys. Rev. E*, **70** (2004), 061907 (7pp).

[25] S. de Franciscis and A. d'Onofrio, Spatiotemporal bounded noises and transitions induced by them in solutions of the real Ginzburg-Landau model, *Phys. Rev. E*, **86** (2012), 021118 (9pp); Erratum, *Phys. Rev. E*, **94** (2016), 0599005(E) (1p).

[26] M. Garavello and B. Piccoli, *Traffic Flow on Networks. Conservation Laws Models*, Amer. Inst. Math. Sci., Springfield, MO, USA, 2006.

[27] G. S. Jiang and C.-W. Shu, Efficient implementation of weighted ENO schemes, *J. Comput. Phys.*, **126** (1996), 202–228.

[28] P. Kachroo, S. J. Al-Nasur, S. A. Wadoo and A. Shende, *Pedestrian Dynamics*, Springer-Verlag, Berlin, 2008.

[29] A. Källén, Thresholds and travelling waves in an epidemic model for rabies, *Nonlin. Anal. Theor. Meth. Appl.*, **8** (1984), 851–856.

[30] A. Källén, P. Arcuri and J. D. Murray, A simple model for the spatial spread and control of rabies, *J. Theor. Biol.*, **116** (1985), 377–393.

[31] Y. Katznelson, *An Introduction to Harmonic Analysis*, Third Ed., Cambridge University Press, Cambridge, UK, 2004.

[32] C. A. Kennedy and M. H. Carpenter, Additive Runge-Kutta schemes for convection-diffusion-reaction equations, *Appl. Numer. Math.*, **44** (2003), 139–181.

[33] W. O. Kermack and A. G. McKendrick, A contribution to the mathematical theory of epidemics, *Proc. Roy. Soc. A*, **115** (1927), 700–721.

[34] N. Kumar, R. R. Parmenter and V. M. Kenkre, Extinction of refugia of hantavirus infection in a spatially heterogeneous environment, *Phys. Rev. E*, **82** (2010), 011920 (8pp).

[35] T. Kuniya, Y. Muroya and Y. Enatsu, Threshold dynamics of an SIR epidemic model with hybrid and multigroup of patch structures, *Math. Biosci. Eng.*, **11** (2014), 1375–1393.

[36] H. N. Liu, L. D. Gao, G. Chowell, S. X. Hu, X. L. Lin, X. J. Li, G. H. Ma, R. Huang, H. S. Yang, H. Tian and H. Xiao, Time-specific ecologic niche models forecast the risk of hemorrhagic fever with renal syndrome in Dongting Lake district, China, 2005–2010, *PLoS One*, **9** (2014), e106839 (8pp).

[37] X.-D. Liu, S. Osher and T. Chan, Weighted essentially non-oscillatory schemes, *J. Comput. Phys.*, **115** (1994), 200–212.

[38] H. Malchow, S. V. Petrovskii and E. Venturino, *Spatial Patterns in Ecology and Epidemiology: Theory, Models, and Simulation*, Chapman & Hall/CRC, Boca Raton, FL, USA, 2008.

[39] J. N. Mills, B. A. Ellis, K. T. McKee, J. I. Maiztegui and J. E. Childs, Habitat associations and relative densities of rodent populations in cultivated areas of central Argentina, *J. Mammal.*, **72** (1991), 470–479.

[40] P. A. P. Moran, Notes on continuous stochastic phenomena, *Biometrika* **37** (1950), 17–23.

[41] J. D. Murray, *Mathematical Biology II: Spatial Models and Biomedical Applications*. Third Edition. Springer, New York, 2003.

[42] J. D. Murray, E. A. Stanley and D. L. Brown, On the spatial spread of rabies among foxes, *Proc. Roy. Soc. London B*, **229** (1986), 111–150.

[43] A. Okubo and S. A. Levin, *Diffusion and Ecological Problems: Modern Perspectives*. Second Edition, Springer-Verlag, New York, 2001.

[44] O. Ovaskainen and E. E. Crone, Modeling animal movement with diffusion, in *S. Cantrell, C. Cosner and S. Ruan (Eds.), Spatial Ecology, Chapman & Hall/CRC,* Boca Raton, FL, USA, 2009, 63–83.

[45] L. Pareschi and G. Russo, Implicit-Explicit Runge-Kutta schemes and applications to hyperbolic systems with relaxation, *J. Sci. Comput.*, **25** (2005), 129–155.

[46] J. A. Reinoso and F. J. de la Rubia, Stage-dependent model for the Hantavirus infection: The effect of the initial infection-free period, *Phys. Rev. E*, **87** (2013), 042706 (6pp).

[47] J. A. Reinoso and F. J. de la Rubia, Spatial spread of the Hantavirus infection, *Phys. Rev. E*, **91** (2015), 032703 (5pp).

[48] R. Riquelme, M. L. Rioseco, L. Bastidas, D. Trincado, M. Riquelme, H. Loyola and F. Valdivieso, Hantavirus pulmonary syndrome, southern chile, 1995–2012, *Emerg. Infect. Dis.*, **21** (2015), 562–568.

[49] C. Robertson, C. Mazzetta and A. d'Onofrio, Regional variation and spatial correlation, *Chapter 5 in P. Boyle and M. Smans (Eds.), Atlas of Cancer Mortality in the European Union and the European Economic Area 1993–1997,* IARC Scientific Publication, WHO Press, Geneva, Switzerland, **159** (2008), 91–113.

[50] E. Rossi and V. Schleper, Convergence of a numerical scheme for a mixed hyperbolic-parabolic system in two space dimensions, *ESAIM Math. Modelling Numer. Anal.*, **50** (2016), 475–497.

[51] S. Ruan and J. Wu, Modeling spatial spread of communicable diseases involving animal hosts, in *S. Cantrell, C. Cosner and S. Ruan (Eds.)*, *Spatial Ecology, Chapman & Hall/CRC, Boca Raton,* FL, USA, 2010, 293–316.

[52] L. Sattenspiel, *The Geographic Spread of Infectious Diseases: Models and Applications*, Princeton Series in Theoretical and Computational Biology, Princeton University Press, 2009.

[53] C.-W. Shu and S. Osher, Efficient implementation of essentially non-oscillatory shock-capturing schemes, II, *J. Comput. Phys.*, **83** (1988), 32–78.

[54] S. W. Smith, *Digital Signal Processing: A Practical Guide for Engineers and Scientists.* Demystifying technology series: by engineers, for engineers. Newnes, 2003.

[55] H. Y. Tian, P. B. Yu, A. D. Luis, P. Bi, B. Cazelles, M. Laine, S. Q. Huang, C. F. Ma, S. Zhou, J. Wei, S. Li, X. L. Lu, J. H. Qu, J. H. Dong, S. L. Tong, J. J. Wang, B. Grenfell and B. Xu, Changes in rodent abundance and weather conditions potentially drive hemorrhagic fever with renal syndrome outbreaks in Xi'an, China, 2005–2012, *PLoS Negl. Trop. Dis.*, **9** (2015), paper e0003530 (13pp).

[56] M. Treiber and A. Kesting, *Traffic Flow Dynamics*, Springer-Verlag, Berlin, 2013.

[57] P. van den Driessche, Deterministic compartmental models: Extensions of basic models, In *F. Brauer, P. van den Driessche and J. Wu (Eds.), Mathematical Epidemiology,* Springer-Verlag, Berlin, **1945** (2008), 147–157.

[58] P. van den Driessche, Spatial structure: Patch models, In *F. Brauer, P. van den Driessche and J. Wu (Eds.), Mathematical Epidemiology*, Springer-Verlag, Berlin, **1945** (2008), 179–189.

[59] P. van den Driessche and J. Watmough, Reproduction numbers and sub-threshold endemic equilibria for compartmental models of disease transmission, *Math. Biosci.*, **180** (2002), 29–48.

[60] E. Vynnycky and R. E. White, *An Introduction to Infectious Disease Modelling*, Oxford University Press, 2010.

[61] J. Wu, Spatial structure: Partial differential equations models, In *F. Brauer, P. van den Driessche and J. Wu (Eds.), Mathematical Epidemiology*, Springer-Verlag, Berlin, 2008, 191–203.

[62] H. Xiao, X. L. Lin, L. D. Gao, X. Y. Dai, X. G. He and B. Y. Chen, Environmental factors contributing to the spread of hemorrhagic fever with renal syndrome and potential risk areas prediction in midstream and downstream of the Xiangjiang River [in Chinese], *Scientia Geographica Sinica*, **33** (2013), 123–128.

[63] C. J. Yahnke, P. L. Meserve, T. G. Ksiazek and J. N. Mills, Patterns of infection with Laguna Negra virus in wild populations of Calomys laucha in the central Paraguayan chaco, *Am. J. Trop. Med. Hyg.*, **65** (2001), 768–776.

[64] W. Y. Zhang, L. Q. Fang, J. F. Jiang, F. M. Hui, G. E. Glass, L. Yan, Y. F. Xu, W. J. Zhao, H. Yang and W. Liu, Predicting the risk of hantavirus infection in Beijing, People's Republic of China, *Am. J. Trop. Med. Hyg.*, **80** (2010), 678–683.

[65] W. Y. Zhang, W. D. Guo, L. Q. Fang, C. P. Li, P. Bi, G. E. Glass, J. F. Jiang, S. H. Sun, Q. Qian, W. Liu, L. Yan, H. Yang, S. L. Tong and W. C. Cao, Climate variability and hemorrhagic fever with renal syndrome transmission in Northeastern China, *Environ. Health Perspect*, **118** (2010), 915–920.

[66] X. Zhong, Additive semi-implicit Runge-Kutta methods for computing high-speed nonequilibrium reactive flows, *J. Comput. Phys.*, **128** (1996), 19–31.

E-mail address: rburger@ing-mat.udec.cl
E-mail address: gchowell@gsu.edu
E-mail address: egavilan@ing-mat.udec.cl
E-mail address: mulet@uv.es
E-mail address: lvillada@ubiobio.cl